

1 **The Capability of Sentinel-MSI (2A/2B) and Landsat-OLI (8/9)** 2 **for Seagrass and Algae Species Differentiation using Spectral** 3 **Reflectance**

4 Abderrazak Bannari ¹, Thamer Salim Ali ² and Asma Abahussain ²

5 ¹Space Pix-Map International Inc., Gatineau (Québec) J8R 3R7, Canada

6 ²Department of Natural Resources and Environment, College of Graduate Studies, Arabian Gulf University, Manama,
7 Kingdom of Bahrain, P.O. Box: 26671, Tel: (973) 1723-9545; Fax: (973) 1723-9552.

8
9 Correspondence to: Abderrazak Bannari, Email: abannari@bell.net

10
11 **Abstract.** This paper assesses the reflectance difference values between the ~~respective spectral bands homologous-in~~
12 ~~the~~ visible and near-infrared (VNIR) ~~spectral bands~~ of Sentinel-MSI-2A/2B and Landsat-OLI-8/9 sensors for seagrass,
13 algae, and mixed species discrimination and monitoring in a shallow marine environment southeastern of Bahrain
14 ~~Island~~ in the Arabian Gulf. To achieve these, a field survey was conducted to collect samples of seawater, underwater
15 sediments, seagrass (*Halodule uninervis* and *Halophila stipulacea*) and algae (green and brown). As well, an
16 experimental mode was established in a Goniometric-Laboratory to simulate the marine environment, and spectral
17 measurements were performed using an ASD spectroradiometer. Measured spectra and their transformation using
18 continuum-removed reflectance spectral (CRRS) approach were analyzed to assess spectral separability among
19 separate or mixed species at varying coverage rates. Afterward, the spectra were resampled and convolved in the solar-
20 reflective spectral bands of MSI and OLI sensors and converted into water vegetation indices (WVI) to investigate the
21 potential of red, green, and blue bands for seagrass and algae species discrimination. The results of spectral and CRRS
22 analyses highlighted the importance of the blue, green, and NIR wavelengths for seagrass and algae detection and
23 likely discrimination based on hyperspectral measurements. However, when resampled and convolved in MSI and
24 OLI bands, spectral information loses the specific and unique absorption features and becomes more generalized and
25 less precise. Therefore, relying on the multispectral bandwidth of MSI and OLI sensors, ~~it~~ is difficult or even
26 impossible to differentiate or to map seagrass and algae individually at the species level. Instead of the red band, the
27 integration of the blue or the green bands in WVI increases their discriminating power of submerged aquatic vegetation
28 (SAV), particularly WAVI, WEVI, and WTDVI indices. These results corroborate the spectral and the CRRS
29 analyses. However, despite the power of blue wavelength to penetrate deeper into the water, it also leads to a relative
30 overestimation of dense SAV coverage due to ~~more the higher~~ scattering in this part of the spectrum. Furthermore,
31 statistical fits ($p < 0.05$) between the reflectance in the VNIR homologous bands of SMI and OLI revealed excellent
32 linear relationships (R^2 of 0.999) with insignificant RMSD (≤ 0.0015). Important agreements ($0.63 \leq R^2 \leq 0.96$) were
33 also obtained between ~~respective homologous~~-WVI regardless of the integrated spectral bands (i.e., red, green, and
34 blue), yielding insignificant RMSD (≤ 0.01). Accordingly, these results pointed out that MSI and OLI sensors are
35 spectrally similar, and their data can be used jointly to monitor accurately the spatial distribution of SAV and it's

36 dynamic in time and space in shallow marine environment, provided that rigorous data pre-processing issues are
37 addressed.

38 1. Introduction

39 Seagrass meadows are identified as an important key for the characterization of environmental resources in estuarine
40 and shallow coastal areas, and a fundamental health index allowing the assessment of coastal ecosystems. The
41 composition and density of their species depend largely on water depth, temperature, salinity, coastal substrate
42 material, and light penetration (Dierssen et al., 2015). Adapted to grow in shallow seawater down to a depth of 20 m,
43 where approximately only 11% of surface light reaches the bottom (Duarte and Gattuso, 2008), they play an essential
44 role in the sustainability of global ecosystem biodiversity in most shallow near-shore areas around the world (Den-
45 Hartog, 1970; Konstantinos *et al.*, 2016). Moreover, the biodiversity of seagrass provides secure habitat and food for
46 a wide variety of marine micro-organisms, improve the quality of water and protect shorelines against erosion in the
47 middle and lower intertidal and sub-tidal zones (Roelfsema *et al.*, 2009; Anders and Lina, 2011; Yang and Yang,
48 2012; Morrison *et al.*, 2014). Like other vegetation cover, seagrass beds play an important role in carbon storage
49 (Novak and Short, 2020), as well as effective removal of carbon dioxide from the “biosphere-atmosphere” system,
50 which significantly mitigates the climate change impacts (Duarte et al., 2013; Lyimo, 2016). Although occupying only
51 0.2% of the world’s oceans (Traganos, 2020), seagrass beds can store twice as much per unit area as forests, and
52 sequester around 10% of the total carbon received by the oceans (Fourqurean et al., 2012).

53 Unfortunately, natural and anthropogenic disturbances and disasters have led to the decline of seagrass around the
54 world (Green and Short, 2003; Orth et al., 2006; Grech et al., 2012; Wood, 2012) at local and regional scales.
55 Undoubtedly, these causes substantially destroy the seagrass beds and biota associated in such habitat and unbalance
56 the ecological functions of coastal zones. Short et al. (2011) showed that seagrass habitat disappeared worldwide at a
57 rate of 110 km² per year between 1980 and 2006. Hence, understanding the spatial distribution of seagrass biomass,
58 its extent, condition, and change over time is essential for their monitoring, management, and protection (Short and
59 Coles, 2001; Waycott *et al.*, 2009). Such monitoring provides updated and accurate information useful for the
60 protection of several ecosystems (Leleu et al., 2012), conservation (Hamel and Andréfouët, 2010), coastal risk
61 assessment (Warren et al., 2016), ecological resources development (Boström et al., 2011), and marine spatial
62 planning (Saarman et al., 2012; Kibele, 2017). In addition, mapping and inventorying the total aboveground biomass
63 of seagrass and algae are important for ecosystem health assessment (Short and Wyllie-Echeverria, 1996), alteration
64 and dynamics in space-time (Neckles et al., 2012), biomass productivity and its contribution to the global biosphere
65 carbon sink capacity (Waycott et al., 2009), and understanding the impacts of climate change (Hashim et al., 2014).

66 In the Arabian Gulf, the extreme environmental conditions combined with major seasonal variations in the marine
67 environment promote the development of three seagrass species including *Halodule uninervis* which is the most
68 dominant species, *Halophila stipulacea* that is less common, and *Halophila ovalis*, which is widely scattered and
69 rarely forms relatively dense meadows. Along the western coast of the Arabian Gulf, these three species are reported
70 and several species of marine algae are described, especially green and brown algae (Erfteimeijer and Shuail, 2012).
71 This natural resource is located in shallow waters with depths ranging from the intertidal zone to 20 m, supporting the

72 second largest population of dugongs (*Dugong dugon*) in the world (Preen, 2004); as well as a large population of
73 Green Turtles (*Chelonia mydas*) and Hawksbill Turtles (*Eretmochelys imbricata*) (Thakur et al., 2007). Unfortunately,
74 these coastal ecosystems are under continuous threats from anthropogenic activities (Waycott et al., 2009), such as
75 reclamation and dredging where several coastal developmental projects are constructed and others under construction
76 (small islands projects development), industrial effluents, oil exploration, pipeline laying, maritime transportation,
77 intensive circulation of commercial fishing boats, pollution and discharges of seawater desalination and wastewater
78 into the sea (Onuf, 1994; Dunton and Schonberg, 2002; Burfeind and Stunz, 2006; Naser, 2011; Erfteimeijer and
79 Shuail, 2012). Eventually, these activities catalyze the degradation and destruction of seagrass species and related
80 ecosystems. Therefore, the assessment of seagrass conditions associated with broad scale of benthic species should be
81 based on relevant and accurate information to measure several health indicators of coastal areas to ensure the
82 sustainable development of these natural resources.

83 Previously, photo-interpretation approaches based on aerial photography have been adopted to follow seagrass and
84 algae species development and assessment in space and time (Ferguson and Wood, 1990; Meehan et al., 2005; Mount,
85 2007). Afterward, the first generation of satellite remote sensing was used to investigate the seagrass classes'
86 composition, differentiation, classification, etc. (Hossain et al., 2014; Komatsu et al., 2020). Unfortunately, these goals
87 were difficult to achieve accurately because the radiometric and spectral resolutions of sensors lacked the sensitivity
88 to discriminate among different marine vegetation species and fragmented classes (Mumby et al., 1997; Wicaksono
89 and Hafizt, 2013). To improve land-water surfaces reflectivity and information extraction, recent developments in
90 remote sensing science and technology have led to an improvement of sensors performance in spatial and spectral
91 resolutions, assuming a potential mapping of the marine environment and aquatic vegetation at the species level;
92 obviously, if species under investigation have distinct spectral signatures. For instance, the Multi-Spectral Instruments
93 (MSI) onboard Sentinel 2A and 2B, as well as the Operational Land Imager (OLI) sensors onboard Landsat 8 and 9
94 platforms were designed with a significant improvement of the signal-to-noise ratio (SNR) and radiometric
95 performances (Knight and Kvaran, 2014). The availability of this new generation of sensors offers innovative
96 opportunities for long-term high-temporal frequency for Earth surfaces' observation and monitoring (Mandanici and
97 Bitelli, 2016). The free availability of their data significantly advances the applications of remote sensing with medium
98 spatial resolutions (Roy et al., 2014; Wulder et al., 2015; Zhang et al., 2018). Thanks to the improvement of their
99 spectral, radiometric, and temporal resolutions, they can expand the range of their applications to several natural
100 resources and environmental domains for monitoring, assessing, and investigating (Hedley et al., 2012a and 2012b).
101 Moreover, the orbits of these four satellites constellation ([Sentinel 2A and 2B and Landsat 8 and 9](#)) are designed to
102 ensure a revisiting interval time of less than 2 days (Li and Roy, 2017; Li and Chen, 2020), thereby substantially
103 increasing the monitoring capabilities of the Earth's surface and ecosystems (Drusch et al., 2012). Their spectral
104 resolutions and configurations are designed in such a way that there is a significant match between the homologous
105 spectral bands, i.e. ~~closely related analogous manner for relative~~ spectral filters position and bandwidths ~~between~~
106 ~~bands~~ (Drusch et al., 2012; Irons et al., 2012). However, depending on the sensitivity of the intended application
107 (Flood, 2017), the sensor radiometric drift calibration (Markham et al., 2016), the atmospheric corrections (Vermote
108 et al., 2016), the surface reflectance anisotropy (Roy et al., 2017), and the sensors co-registration (Skakun et al., 2017;

109 Yan et al., 2018), it is plausible that the natural surface-reflectances recorded by MSI and OLI sensors over the same
110 target in the marine environment may be different. In addition, the relative spectral response profiles characterizing
111 the filters (spectral responsivities) of these instruments are not perfectly identical between the homologous bands, so
112 some differences are probably expected over the recorded land or water surfaces reflectance values and, therefore,
113 their data cannot be reliably used together (Bannari et al., 2004; Van-derWerff and Van-der-Meer, 2016; Bannari,
114 2019). The importance of these differences depends on the application (spectral characteristics of the observed target)
115 and on the approach adopted to perform time-series analyses, mapping, or change detection exploiting these
116 instruments (Flood, 2017). For instance, it is plausible that the extraction of seagrass and/or algae information in time
117 over shallow water areas using surface reflectances, empirical, semi-empirical, and/or physical approaches, may affect
118 the comparison of the results.

119 The main objectives of this research focus on the analysis of Sentinel-MSI and Landsat-OLI homologous visible
120 and near-infrared (VNIR) bands capability to distinguish and discriminate among seagrass (*Halodule uninervis* and
121 *Halophila stipulacea*), algae (green and brown), and any probable case of mixed species of seagrass and algae sampled
122 from the southeast area of Bahrain national water. To achieve these, the specific following steps are considered. 1)
123 Examination of spectral signatures in VNIR wavelengths and their continuum-removal transformations for potential
124 differentiation among the considered seagrass and algae species and their mixture submerged in seawater at different
125 coverage rates, as well as considering the sediment-substrate with ~~bright clear~~ and dark colors. 2) Comparison and
126 analysis of the difference between the resampled and convolved reflectances in the VNIR homologous bands of MSI
127 and OLI sensors considering all examined samples. 3) Comparison between MSI and OLI sensors in terms of
128 converting the reflectances over the considered samples at different coverage rates into several water vegetation
129 indices (WVI). Finally, 4) efficiency and accuracy analysis of the examined WVI to discriminate between species
130 (seagrass, algae and mixed) by integrating the green and blue bands instead of the red band. Further, according to
131 these analyses results, it will be clear whether it possible for these sensors to differentiate between seagrass and algae
132 effectively and precisely at the species level, or simply and generally to discriminate among submerged aquatic
133 vegetation (SAV) cover at different density classes. Moreover, to place this research in the international context, the
134 following section reviewed the use of remote sensing (sensors and methods) for the detection, discrimination and
135 mapping of different seagrass and algal species in many coastal locations around the world.

136 2. Remote sensing of seagrass and algae detection and mapping: A review

137 Traditional seagrass *in-situ* surveys require time and intensive field sampling, which is generally lack the spatial
138 coverage and precision that are required to detect changes before they become irreversible or very difficult to maintain
139 year after year (Peterson and Fourqurean, 2001; Yang and Yang, 2012). Over the recent decades, remote sensing
140 science and sensors technology has played an essential role in seagrass mapping and monitoring (Dean and Salim,
141 2013; Dierssen et al., 2015). According to literature, the mapping of the characteristics and properties of seagrass and
142 algae in the marine environment occurs over relatively small areas with limited variations in water depth and clarity
143 using satellite, airborne, and drone remote sensing sensors (multispectral and hyperspectral). Moreover, field and

144 laboratory *in-situ* measurements have been conducted for calibration and validation in several environments around
145 the world (Larkum *et al.*, 2006; Roelfsema *et al.*, 2009; Hossain *et al.*, 2014; Komatsu *et al.*, 2020; Duffy *et al.* 2018).

146 Under laboratory conditions using spectral measurements, Thorhaug *et al.* (2007) demonstrated the near similarity
147 in the shape and form of the spectral signatures of three different seagrass species with a very slight difference and
148 pointed out subtle differences between marine algae (green and brown) and seagrass. In the central west coast of
149 Florida in the USA, Pu *et al.* (2012) used *in-situ* Hyperspectral measurements in the field and laboratory to analyse
150 the spectral behaviour and the potential discrimination among several seagrass species according to their spatial extent
151 and abundance, water depths, and substrate types. They highlighted that the discrimination of seagrass species and the
152 percentage of SAV coverage are affected by water depth and substrate on the measured spectra. Moreover, Wood
153 (2012) demonstrated the potential of the synergy between the field spectra and hyperspectral data for seagrass sensing
154 and mapping in Redfish Bay, Texas in the USA. Exploiting modeled and simulated data, Hedley *et al.* (2012a)
155 demonstrated that Sentinel-MSI has an improved capability for detection and discrimination of the marine
156 environment compared to SPOT-4 and Landsat-ETM+. Furthermore, Fyfe (2003) reported that the spectral signatures
157 measured on harvested wet leaves (out of water) of different seagrass species were spectrally distinct. However, the
158 real marine environment conditions are different from wet leaves due to water-column constituents including
159 phytoplankton, suspended organic and inorganic matter, water depth variability, and optical properties of the
160 underlying sediments (Pu *et al.*, 2012).

161 Otherwise, NASA's Landsat program is the earliest and most commonly used over the past five decades. It consists
162 of a series of nine satellite missions using four types of multispectral sensors including MSS, TM, ETM +, and OLI
163 (Bannari and Al-Ali, 2020). These sensors have been used by many scientists to detect and map seagrass beds at local
164 and regional scales (Phinn *et al.* 2008; Knudby and Nordlund, 2011; Lyons *et al.* 2012 and 2013; Kovacs *et al.* 2018).
165 Exploring a time-series of 23 annual images acquired over the Eastern Banks of Moreton Bay in Australia, Lyons *et*
166 *al.* (2013) demonstrated how TM and ETM+ data time-series analysis enabled seagrass spatial distribution to be
167 appropriately assessed spatiotemporally. Moreover, a regional-scale mapping of seagrass habitat in the Wider-
168 Caribbean region was achieved with acceptable accuracies using a total of 40 scenes acquired with TM and ETM+
169 sensors, and applying different images processing methods (Wabnitz *et al.*, 2008). In Cam-Ranh Bay in Vietnam,
170 Chen *et al.* (2016) investigated the temporal changes of seagrass beds over 20 years (1996 to 2015) by exploiting
171 multi-temporal Landsat data acquired with TM, ETM+ and OLI sensors. Dekker *et al.* (2005) demonstrated that TM
172 and ETM+ instruments did not have sufficient spectral and radiometric resolutions to discriminate among three
173 seagrass species in a shallow coastal Australian lake. Contrariwise, Dahdouh-Guebas *et al.* (1999) reported the utility
174 of TM data associated with ground truth measurements to map accurately the distribution of seagrass and algae on the
175 Kenyan coast. In addition to the Landsat sensor series, the European satellites such as SPOT-HRV were also used in
176 combination with *in-situ* spectroradiometric measurements and quantitative semi-empirical models to assess the
177 changes in the spatial distribution of seagrass biomass in Bourgneuf-Bay in France over 14 years (Barillé *et al.* 2010).
178 Likewise, the potential of the Indian satellite (IRS-ID LISS-III) has been demonstrated for mapping the seagrass
179 meadows extent in the Gulf of Mannar Biosphere Reserve in India (Umamaheswari *et al.*, 2009).

180 Furthermore, the first generation of commercial satellites operated by the private remote sensing industry with
181 very high ~~spatial resolution pixel size~~ and narrow spectral resolutions, such as IKONOS, Quickbird, WorldView, etc.,
182 offers complementary technology for seagrass sensing and mapping. This new technology provides an excellent
183 compromise between spatial and spectral resolutions for information extraction. In clear water seagrass habitat in the
184 Moreton-Bay (Australia), the spatial and temporal dynamics of seagrasses (cover, species, and biomass) have been
185 studied from the leaf to patch scales between 2004 and 2013 integrating nine high spatial resolutions images acquired
186 with WorldView-2, IKONOS, and Quickbird-2 and applying object-image processing approach (Roelfsema *et al.*,
187 2014). The results showed the utility of this new spatial technology for time-series analysis and the derivation of
188 seagrass products that are very useful in marine ecology management. Moreover, Knudby and Nordlund (2011)
189 highlighted the utility of IKONOS data for multi-species of seagrass detection in a patchy environment around
190 Chumbe Island in Zanzibar (Tanzania). Along Zakynthos Island in Greece, Pasqualini *et al.* (2005) demonstrated that
191 the SPOT-5 data with 2.5 and 10 m spatial resolutions are suitable for seagrass classes' classification according to the
192 overall accuracies. In shallow waters of Moreton Bay in Australia, Phinn *et al.* (2008) have shown that the spatial and
193 spectral resolutions of multispectral (Quickbird and Landsat-TM) and hyperspectral (airborne CASI) data affects the
194 precision of seagrass biomass differentiation at the species level, i.e., when the pixel size increases the error is getting
195 higher. Contrary to these findings, in the Capo Rizzuto area in Italy, Dattola *et al.* (2018) reported the potential of the
196 high spatial resolution of WorldView-2 compared to the medium resolution of MSI and OLI for different seagrass
197 species characterization. In addition, to identify the spatial distribution of seagrass beds in Xincun Bay (Hainan
198 province in China), Yang and Yang (2009) demonstrated that Quickbird data are more accurate than those of TM and
199 CBERS (China-Brazil Earth Resources Satellite data) sensors.

200 In addition to remote sensing sensor technologies, a variety of image processing methods have been employed in
201 mapping seagrass spatial distribution and coverage. For instance, Marcello *et al.* (2018) demonstrated the good
202 performance of support vector machines (SVM) approach compared to spectral angle mapper (SAM) and maximum
203 likelihood for seagrass classification; moreover, they pointed out the greater aptitude of hyperspectral compared to
204 multispectral data. Likewise, Peneva *et al.* (2008) reported that the maximum likelihood classification produced the
205 highest overall accuracy while SAM yielded the lowest accuracy due to the predominant influence of water-column
206 optical properties on the apparent spectral characteristics of seagrass and sand bottom in the northern Gulf of Mexico.
207 For *Posidonia oceanica* mapping in the Mediterranean region, the random forests method gives more accurate results
208 than SVM approaches when compared with in-situ observations (Bakirman and Gumusay, 2020). Whereas, using a
209 high spatial resolution of WorldView-2 imagery acquired over a coastal area in Florida, the neural network classifier
210 performed better than SVM for seagrass mapping (Perez *et al.*, 2020). According to Uhrin and Townsend (2016),
211 linear spectral mixture analysis (LSMA) can be used with photo interpretation to generate spatially resolved maps
212 suitable for seagrass spatial distribution and provide improved estimates of seagrass classes. Nevertheless, Chen *et al.*
213 (2016) revealed the difficulty and limitation of LSMA for mapping the fraction of scattered and heterogeneous
214 seagrass patches that are smaller than the pixel size. At Ritchie's archipelago within the Andaman and Nicobar group
215 of Islands, Bayyana *et al.* (2020) showed that Sentinel-MSI data can detect, and map submerged benthic habitat and
216 seagrass beds present at a depth of 21 m using random forest, SVM, and K-nearest-neighbour classification algorithms.

217 Besides, linear regressions were established between the field truth measurements and several vegetation indices
218 derived from SPOT-XS, Landsat-TM, and CASI Hyperspectral airborne, to measure the density of seagrass in the
219 tropical Western Atlantic (Mumby et al., 1997).

220 Since the emergence of remote sensing as a new scientific discipline in the early 1970s, vegetation indices (VI's)
221 were involved as radiometric measurements of the spatial and temporal distribution of land vegetation photo-
222 synthetically active. They use the red and near-infrared (NIR) bands, the normalized difference vegetation index
223 (NDVI) was proposed by Rouse et al. (1974) at the dawn of remote sensing. Since these two spectral bands are
224 generally present on Earth observation and meteorological satellites, and often containing more than 90% of the
225 information relating to vegetation canopy (Bannari et al., 1995), the NDVI had taken a privileged place in the
226 NASA/NOAA Pathfinder project (James and Kalluri, 1994). Thus, it was daily derived from NOAA-AVHRR data at
227 the Earth scale. Subsequently, it was also derived every day from MODIS and SPOT-Vegetation data to produce time-
228 series products for global vegetation assessment and monitoring at the regional and global scales. Due to this glorious
229 history and its simplicity, the NDVI has become the most widely used to assess vegetation canopy. Then, this index
230 was improved in a new version named soil adjusted vegetation index (SAVI) by Huete (1988) to minimize the artefacts
231 caused by soil background on the estimation of vegetation cover fraction by incorporating a correction factor "L". To
232 overcome the limitations of linearity and saturation, to reduce the noise of atmospheric effects, and to remove the
233 artefacts of soil optical properties, the enhanced vegetation index (EVI) was proposed also by Huete *et al.* (2002).
234 Likewise, the transformed difference vegetation index (TDVI) was developed by Bannari *et al.* (2002) to describe the
235 vegetation cover fraction independently to the background artefacts, to reduce the saturation problem, and to enhance
236 the vegetation dynamic range linearly. These indices (NDVI, SAVI, EVI, and TDVI) were used to establish a close
237 relationship between radiometric responses and land vegetative cover densities, and they were implemented in the
238 ENVI image processing system.

239 In marine applications, several scientists for seagrass and algae discrimination and mapping tested these indices.
240 The NDVI extracted from SPOT-HRV images coupled with *in-situ* spectroradiometric data provided satisfactory
241 results for spatiotemporal change of seagrass beds in Bourgneuf-Bay in France (Barillé et al., 2009). Using
242 hyperspectral data, Dierssen et al. (2015) reported the potential of NDVI for SAV classes' discrimination. Similarly,
243 Zoffoli et al. (2020) demonstrated the capability of NDVI derived from Sentinel-MSI data for seagrass percent cover
244 estimation and leaf biomass mapping to characterize its seasonal dynamics along the European Atlantic coast.
245 However, although VNIR bands are generally available in optical remote sensing satellites, it is well known that only
246 the visible bands can penetrate ocean water deeper than NIR which is largely absorbed by the water surface (Kirk,
247 1994). Thus, regardless of the concentrations of suspended sediments and/or organic matter, the visible wavelengths
248 are used to map the marine environment. Indeed, the blue penetrates deeper (~ 37 m) than any other wavelengths,
249 followed by green (~ 30 m), then red (~ 7 m), and NIR (Fig. 1) penetrates the least, being attenuated in the shallowest
250 depths around 2.5 m (Komatsu et al., 2020). Accordingly, blue, green, and red are the most suitable for sensing
251 seagrass and SAV (Silva et al., 2008). Thereby, when vegetation indices are applied in the marine environment
252 (Davranche et al., 2010; Zhao et al., 2013), always the red band is substituted by that of blue or green. Then, discussion
253 was initiated on WVI or aquatic vegetation indices (AVI). For instance, when the red was replaced by the green in

254 NDVI (Yang and Yang, 2009) and by the blue in SAVI (Villa et al., 2013) these versions were named, respectively,
 255 the Normalized Difference Aquatic Vegetation Index (NDAVI or WNDVI) and Water Adjusted Vegetation Index
 256 (WAVI). These two new versions were found more sensitive to seagrass LAI and percentage cover density, and
 257 discriminated better among species of seagrass (Yang and Yang, 2009; Villa et al., 2013). To separate and map
 258 vegetation features over some lake ecosystems in Italy, the NDAVI and the WAVI performed suitably (Villa et al.,
 259 2014). As well, for open water features delineation, Mcfeeters (1996) replaced the difference between “NIR and red”
 260 in the NDVI with that between “green and NIR”, and he baptised this new combination the Normalized Difference
 261 Water Index (NDWI). In Taihu and Duck Lakes in China, NDVI and NDWI were used for wetland and SAV pattern
 262 delineation and classification (Lin et al., 2010; Zhao et al., 2013). Likewise, the visible atmospherically resistant index
 263 (VARI) was proposed by Gitelson et al. (2002a) to estimate the green vegetation fraction. While the triangular
 264 greenness index (TGI) was developed by Hunt et al. (2013) based on the chlorophyll absorption features. The
 265 capability of VARI and TGI was examined by Li (2018) who highlighted the advantage of VARI compared to TGI
 266 for seagrass biomass mapping in Core Banks in North Carolina in the USA. Proposed by Richardson and Wiegand
 267 (1977), the difference vegetation index (DVI) provided satisfactory results for mangrove cover and carbon stock
 268 estimation in the estuary and marine environment (Candra et al., 2016). Moreover, the difference-index between the
 269 blue and the green bands (DIF-BG) showed the best fits between observed and predicted SAV as reported by Mumby
 270 et al. (1997).

271

272

[Figure 1]

273 3. Materials and Methods

274 Fig. 2 illustrates the followed methodology, which is based on a field survey to collect samples including seawater,
 275 sediments, seagrass (*Halodule uninervis* and *Halophila stipulacea*) and algae (green and brown) from shallow marine
 276 environment at different depths (0.50 to 7 m) of southeast Bahrain Island. To simulate the marine environment, an
 277 experimental mode was established in a Goniometric-Laboratory and spectral measurements were performed using
 278 an Analytical Spectral Devices (ASD) spectroradiometer over each separate and mixed species at different coverage
 279 rate (0, 10, 30, 75, and 100%), as well as simulating the seabed with dark and bright clear-colors. To assess the spectral
 280 signatures variability that can be found among each separate or mixed species at varying coverage rates, all measured
 281 spectra were analyzed and transformed using continuum-removed reflectance spectral (CRRS) approach (see section
 282 3.4). Then, the spectra were resampled and convolved in the solar-reflective spectral bands of MSI and OLI sensors
 283 using the *Canadian Modified Simulation of a Satellite Signal in the Solar Spectrum* (CAM5S) (Teillet and Santer,
 284 1991) based on Herman radiative transfer code (RTC), and the relative spectral response profiles characterizing the
 285 filters of each instrument in the VNIR bands. Afterward, convolved spectra were converted into several WVI
 286 integrating the red, green, and blue bands. For comparison and sensor differences quantification, statistical fits were
 287 conducted using linear regression analysis ($p < 0.05$) between reflectances in homologous bands and between the
 288 examined homologous WVI derived from the two sensors data considering all samples, i.e., seawater, sediments,
 289 seagrass, and algae species (individually and mixed at the considered coverage rates). The coefficient of determination

290 (R^2), difference values, and root mean square difference (RMSD) were calculated for reflectances and all versions of
291 investigated WVI's.

292

293 [Figure 2]

294 3.1. Study Site

295 The area under investigation in this research is the water boundary of the Kingdom of Bahrain (25° 32' and 26°00'N,
296 50° 20' and 50° 50'E) which is a group of islands located in the Arabian Gulf, east of Saudi Arabia and west of Qatar
297 (Fig. 3). The archipelago comprises 33 islands, with a total area of 8269 km², 9% of it is a land area (778.4 km²).
298 Along the southeast coast of Bahrain, the continental plateau extends for kilometers with a depth of less than one or
299 two meters. The main island of Bahrain is surrounded by shoal areas named "Fashts" where depths do not exceed 10
300 m (Bannar i and Kadhem, 2018). These areas generally support a variety of species of seagrass, algae, coral, and
301 fishes. Moreover, they play an important role in the hydrodynamic regime, which supports diverse biological
302 ecosystems. Fig. 3 also illustrates the reclamation and dredging operations that have occurred in the study area over
303 the past three decades where several coastal developmental projects are constructed, and others are in progress. These
304 anthropogenic activities strongly contribute to the degradation and even to the destruction of seagrass species and
305 associated coastal ecosystems.

306

307 [Figure 3]

308 3.2. Field sampling

309 Seagrass and algae samples were collected on 4th May 2017 from different meadows locations, which are characterized
310 by a depth range from 0.5 to 7 m in the south and southeast waters of Bahrain (Fig. 4a). Some locations were dominated
311 with *Halodule uninervis* (HU), others scattered, ~~and others were or densely patches were a mixed ture~~ between HU
312 and *Halophila stipulacea* (HS). HU is the most dominant species (Fig. 4b), it occurs as dense or scattered meadows
313 patches along shoreline (Erftemeijer and Shail, 2012). This species is like grass with narrow leaves (around 3 mm in
314 width and 25 cm in length). Whereas, HS (Fig. 4c) has darker green leaves reaching 10 cm in length and it is widely
315 present in the Arabian Gulf. The brown (BA, Fig. 4d) and green (GA, Fig. 4e) algae were accessible near to shores
316 and shallow water in general. In addition to the sediments (Fig. 4f) and pure seawater samples, which were collected
317 separately, samples of each seagrass and algae species were selected and harvested in healthy and fresh conditions
318 from several stations within the study area. Then, they were stored separately in non-translucent plastic bags with
319 seawater and immediately placed in a cooler for transportation from the field to the laboratory. This was done to
320 prevent structural and leaf pigment damages due to the delay between sampling time and spectroradiometric
321 measurements in the Goniometric-Laboratory.

322

323 [Figure 4]

324 3.3. Spectroradiometric measurements

325 Spectroradiometric measurements were acquired in a dark BRDF Goniometric-Laboratory above each sample
326 separately, then above ~~d~~-and-mixed samples (Fig. 5), using an ASD spectroradiometer (ASD Inc., 2015). This
327 instrument is equipped with two detectors operating in the VNIR and shortwave-infrared (SWIR), between 350 and
328 2500 nm. It acquires a continuous spectrum with a 1.4 nm sampling interval from 350 to 1000 nm and 2 nm from
329 1000 to 2500 nm. The ASD resamples the measurements in 1-nm intervals, which allows the acquisition of 2151
330 contiguous hyperspectral bands per spectrum. The sensor is characterized by the programming capacity of the
331 integration time, which allows an increase of the SNR and stability. The data were acquired at nadir with a field of
332 view (FOV) of 25° and a solar zenith angle of approximately 5° by averaging 40 measurements. The ASD was installed
333 on a BRDF Goniometric-System with a height of approximately 65 cm over the target, which makes it possible to
334 observe a surface of ~ 830 cm². A laser beam was used to locate the center of the ASD-FOV. The reflectance factor
335 of each sample was calculated by rationing target radiance to the radiance obtained from a calibrated “Spectralon
336 panel” according to the method described by Jackson et al. (1980). Moreover, the corrections were applied for the
337 wavelength dependence and non-lambertian (i.e. uneven light distribution in all directions) behavior of the panel
338 (Sandmeier et al., 1998; ASD, 2015; Ben-Dor et al., 2015). The measurements were carried out above each collected
339 sample including seawater, sediments, seagrass, and algae species as well as mixed species (seagrass and algae)
340 considering different coverage rates (0, 10, 30, 75, and 100%). Each sample was placed and measured twice in black
341 and ~~clear~~-bright (yellow) large bowls, considering two sedimentary substrates (dark and ~~clear~~-bright) underlying the
342 seagrass and algae samples that were submerged by seawater, i.e., simulating the aquatic environment. Since the
343 remote sensing of benthic aquatic vegetation is mostly limited to the VNIR ranges (Fig. 1) only the wavelengths
344 interval between 400 and 1000 nm are considered in our analyses.

345

346 [Figure 5]

347 3.4. Continuum-removed reflectance spectral (CRRS) transformation

348 Spectral signatures are processed and transformed using numerous approaches to retrieve information about change
349 in absorption features (position, depth, width, and asymmetry) of a particular target over a specific bandwidth between
350 350 and 2500 nm (Van-Der-Meera, 2004). To emphasize these absorption features, many approaches were proposed
351 including relative absorption-band-depth (Crowley et al., 1989), spectral feature fitting technique, and Tricorder and
352 Tetracorder algorithms (Clark et al., 2003). These approaches work on the so-called CRRS approach, thus recognizing
353 that the absorption in a spectrum has a continuum and individual absorption features (Clark *et al.*, 1987; Van-Der-
354 Meera, 2004; Clark *et al.*, 2014). Proposed by Clark and Roush (1984), CRRS transformation and analysis allows the
355 isolation of individual absorption features in the hyperspectral signature of a specific target under investigation,
356 analysis, and comparison. It normalizes the original spectra and helps to compare individual absorption features from
357 a common baseline (Clark *et al.*, 1987). The continuum is a convex hull fit over the top of a spectrum under study
358 using straight-line segments that connect local spectra maxima. The first and last spectral data values are on the hull;
359 therefore, the first and last bands in the output continuum-removed data file are equal to 1.0. In other words, after the

360 continuum is removed, a part of the spectrum without absorption features will have a value of 1, whereas complete
361 absorption would be near to 0, and with most absorptions falling somewhere in between. The CRRS approach was
362 used for discriminating and mapping rocks mineralogy (Clark et al., 1990; Clark and Swayze, 1995), land vegetation
363 cover (Kokaly et al., 2003; Huang et al., 2004; Manevski et al., 2011), and seagrass and SAV (Barillé et al., 2011;
364 Bargain et al., 2012; Wicaksono et al., 2019; Indayani et al., 2020). In this study, the continuum algorithm
365 implemented in the ENVI image processing system was used (ENVI, 2012).

366 3.5. Spectral sampling and convolving in MSI and OLI spectral bands

367 Since 1972, the Landsat scientific collaboration program between NASA and USGS constitutes the continuous record
368 of the Earth's surface reflectivity from space. Indeed, the Landsat satellites series support five decades of a global
369 medium spatial resolution data collection, distribution, and archive of the Earth's surfaces (Bannari et al., 2004;
370 Loveland and Dwyer, 2012) to support research, applications, and climate change impacts analysis at the global, the
371 regional and the local scales (Roy et al., 2014 and 2016; Wulder et al., 2015). Benefiting from the acquired space-
372 engineering experience, from the heritage of Landsat instruments, and the advanced development of technology during
373 the last five decades, the fourth generation of Landsat is composed of two similar sensors with very high spectral and
374 radiometric sensitivities: OLI-1 and OLI-2 (Markham et al., 2016; Li and Chen, 2020). The OLI-1 carried onboard
375 Landsat-8 was launched on 11th February 2013, and OLI-2 onboard Landsat-9 was launched on 27th September 2021
376 (NASA, 2019 and 2021). The OLI sensors collect land-surface reflectivity in the VNIR, SWIR, and panchromatic
377 wavelength with a FOV of 15° covering a swath of 185 km with 16 days' time repetition at the equator. The band
378 passes are narrower to minimize atmospheric absorption features (NASA, 2014), especially the NIR spectral band
379 (0.865 µm). Two new spectral bands have been added: a deep blue visible shorter wavelength (band 1: 0.433 - 0.453
380 µm) designed specifically for water resources and coastal zone investigation and a new SWIR band (9: 1.360 - 1.390
381 µm) for the detection of cirrus clouds. Moreover, compared to previous TM and ETM+ sensors using only 8 bit, the
382 OLI design results in more sensitive instruments with a significant improvement of the SNR radiometric performance
383 quantized over a 12-bit dynamic range (Level 1 data), and raw data are delivered in 16 bit. The high performance of
384 SNR associated with improved radiometric and spectral resolutions provide a superior dynamic range of radiance by
385 reducing saturation problems and, therefore, enabling better characterization of land and water surface conditions
386 (Knight and Kvaran, 2014), especially with orbit reflective radiometric calibration better than 3% (Markham et al.,
387 2014; Gascon et al., 2017). Table 1 summarizes the effective bandwidth characteristics of OLI-1 and OLI-2 sensors.

388

389

[Table 1]

390

391 Otherwise, the Sentinel-2 mission is the result of close collaboration between the European Space Agency, the
392 European Commission, industry, service providers, and data users. It is composed of two satellites, Sentinel 2A and
393 2B that were launched in June 2015 and in March 2017, respectively. Both satellites are equipped with identical MSI
394 sensors to provide continuity to the SPOT missions and to improve the Landsat-OLI temporal frequency (Drusch et
395 al., 2012). The synergy between the four sensors (MSI-2A, MSI-2B, OLI-1, and OLI-2) significantly increase the

396 temporal resolution (around 2 days) offering new opportunities for several environmental and natural resource
 397 applications, such as the vigour of vegetation cover, emergency management, water quality, seagrass meadows, and
 398 climate change impacts analysis at local, regional, and global scales. The MSI images the Earth's surface reflectivity
 399 with a large FOV (20.6°) in 13 spectral bands with several spatial resolutions from 10 to 60-m; four bands with 10-m
 400 (blue, green, red, and NIR-1), six bands with 20-m (Red-Edge, NIR-2, and SWIR), and three bands with 60-m (coastal,
 401 water vapor and cirrus). The swath of each scene is 290 km, permitting global coverage of the Earth's surface every
 402 10 days. The MSI radiometric performance is coded in 12 bits, ensuring radiometric calibration accuracy of better
 403 than 3% and an excellent SNR (Markham et al., 2014; Li et al., 2017). Table 1 summarizes the effective bandwidth
 404 characteristics of MSI-2A and MSI-2B sensors.

405 As discussed above, the measured bidirectional reflectance factors with the ASD have a 1-nm interval allowing
 406 the acquisition of 2151 contiguous hyperspectral bands per spectrum. However, most multispectral remote sensing
 407 instruments measure integrated reflectance over broad bands (equation 1). Consequently, the average of 40 spectra
 408 measured with the ASD over each sample was resampled and convolved to match the solar-reflective spectral
 409 responses functions characterizing the optics and electronics of MSI and OLI instruments in the VNIR spectral bands
 410 (Fig. 6). In this step, the resampling procedure considers the nominal width of each spectral band (Table 1). Then, the
 411 convolution process was executed using the CAM5S transfer radiative code (Teillet and Santer, 1991). This
 412 fundamental step simulates the signal received by the considered sensors at the top of the atmosphere from a surface
 413 reflecting solar and sky irradiance at sea level, considering the filter of each band (Fig. 6), and assuming ideal
 414 atmospheric conditions without scattering or absorption (Zhang and Roy, 2016). Accordingly, the equivalent
 415 convolved reflectance ($\rho(\lambda_i, \lambda_s)_i$) over each sample was generated at the satellite orbit altitude in homologous VNIR
 416 spectral bands of each sensor (Slater, 1980):

$$417 \rho(\lambda_i, \lambda_s)_i = \frac{\int_{\lambda_i}^{\lambda_s} R(\lambda) \cdot S(\lambda)_i \cdot d(\lambda)}{\int_{\lambda_i}^{\lambda_s} S(\lambda)_i \cdot d(\lambda)} \quad (1)$$

419 Where $\rho(\lambda_i, \lambda_s)_i$ is the equivalent convolved reflectance of the band “i” of each sensor, λ_i to λ_s are the spectral
 420 wavelength ranges of the band “i” of each sensor, $R(\lambda)$ is the corresponding reflectance at wavelength “ λ ” measured
 421 by the ASD, and $S(\lambda)_i$ is the corresponding spectral responsivity value of the spectral response function of the band
 422 “i” of each sensor (Fig. 6). It is important to note that the MSI-NIR-2 broadband (band-8: 785 - 900 nm) is not
 423 considered in this study because it is not a real homologous band of OLI-NIR, and it has a greatest reflective band
 424 difference with the OLI-NIR (851–879 nm). The OLI-NIR spectral response function intersects with only 20% of the
 425 MSI-NIR-2 response function. Moreover, the MSI red-edge bands were not considered also as they are not acquired
 426 by the OLI sensor.

428

429

[Figure 6]

430 3.6. Data Processing

431 In addition to remote sensing sensor technologies' improvement and innovation, a variety of processing methods have
 432 been applied for spectral data for mapping and monitoring seagrass and habitats in shallow coastal waters. They were
 433 applied to highlight the seagrass and algae species composition, leaf area index estimation, percentage cover mapping,
 434 etc. They include matched filtering approach (Li et al., 2012), object-based image analysis (Roelfsema *et al.*, 2014),
 435 adaptive coherence estimator and constrained energy minimization (Li et al., 2012), artificial neural network model
 436 (Perez et al., 2020), linear spectral mixture analysis (Uhrin and Townsend, 2016; Chen et al., 2016), spectral angle
 437 mapper (Peneva et al., 2008; Li et al., 2012; Marcello et al., 2018; Wicaksono et al., 2019), classification tree analysis
 438 (Wicaksono et al., 2019), random forest (Bayyana et al., 2020), support vector machines (Marcello et al., 2018;
 439 Bakirman and Gumusay, 2020; Perez et al., 2020; Bayyana et al., 2020), and machine learning regression (Traganos,
 440 2020; Bakirman and Gumusay, 2020). Undeniably, these sophisticated and complicated methods require extensive
 441 training information and field endmember measurements. However, the simplicity of empirical and semi-empirical
 442 methods based on vegetation indices are easier to transfer between sensors and can be used as a robust alternative
 443 compared to the complex processing methods; because these methods are based on the knowledge of spectral
 444 absorption features that characterize specifically the target under investigation. Moreover, these methods have the
 445 advantage of being reproducible, easily transferable, and applicable in other geographic regions. Each method has
 446 advantages and limitations, especially in shallow water. In this study, after the spectral analysis and CRRS
 447 transformation, the capability and comparison of the VNIR homologous spectral bands of MSI and OLI sensors were
 448 investigated for seawater, sediments, seagrass, algae, and mixed species discrimination at different coverage rates.
 449 Then, although the literature refers to more than fifty vegetation indices for land vegetation cover monitoring and
 450 characterization (Bannari et al., 1995), only the most popular indices that have been used for seagrass and SAV in
 451 different marine environments around the world were retained in this study. After spectral data pre-processing,
 452 sampling, and convolving, the indices TGI, VARI, and Diff(G-B) were implemented and tested respecting their
 453 original and unchangeable equations. While the NDVI, SAVI, EVI, TDVI, NDWI, and DVI indices were calculated
 454 in three versions by integrating the red, blue, and green bands. The equations of the considered indices are as follow:

$$455 \text{NDVI} = (\rho_{\text{NIR}} - \rho_{\text{Red}}) / (\rho_{\text{NIR}} + \rho_{\text{Red}}) \quad (\text{Rouse et al., 1974}) \quad (2)$$

$$456 \text{SAVI} = 1.5 * (\rho_{\text{NIR}} - \rho_{\text{Red}}) / (\rho_{\text{NIR}} + \rho_{\text{Red}} + 0.5) \quad (\text{Huete, 1988}) \quad (3)$$

$$457 \text{TDVI} = 1.5 * (\rho_{\text{NIR}} - \rho_{\text{Red}}) / (\sqrt{(\rho_{\text{NIR}}^2 + \rho_{\text{Red}} + 0.5)}) \quad (\text{Bannari et al., 2002}) \quad (4)$$

$$458 \text{NDWI} = (\rho_{\text{Green}} - \rho_{\text{NIR}}) / (\rho_{\text{Green}} + \rho_{\text{NIR}}) \quad (\text{McFeeters, 1996}) \quad (5)$$

$$459 \text{EVI} = 2.5 * (\rho_{\text{NIR}} - \rho_{\text{Red}}) / (\rho_{\text{NIR}} + 6 * \rho_{\text{Red}} - 7.5 * \rho_{\text{Blue}} + 1) \quad (\text{Huete et al., 2002}) \quad (6)$$

$$460 \text{DVI} = \rho_{\text{NIR}} - \rho_{\text{Red}} \quad (\text{Richardson and Wiegand, 1977}) \quad (7)$$

$$461 \text{VARI} = (\rho_{\text{Green}} - \rho_{\text{Red}}) / (\rho_{\text{Green}} + \rho_{\text{Red}} - \rho_{\text{Blue}}) \quad (\text{Gitelson et al., 2002a}) \quad (8)$$

$$462 \text{TGI} = \rho_{\text{Green}} - 0.39 * \rho_{\text{Red}} - 0.61 * \rho_{\text{Blue}} \quad (\text{Hunt et al., 2013}) \quad (9)$$

$$463 \text{Diff(G-B)} = \rho_{\text{Blue}} - \rho_{\text{Green}} \quad (\text{Mumby et al., 1997}) \quad (10)$$

464

465
 466 The wavelength ranges of the used VNIR bands for Sentinel-MSI and Landsat-OLI are summarize in Table 1.

467 3.7. Statistical analyses

468 As discussed previously, the respective MSI and OLI ~~relative~~-spectral response profiles characterizing the filters of
 469 each spectral band differ somewhat ~~are relatively different~~ (Fig. 6). To examine the impact of this difference, statistical
 470 analyses were computed using “Statistica” software. The relationships between the product values (reflectances and
 471 WVI’s) derived from MSI against those obtained from OLI were analyzed between homologous bands using a linear
 472 regression model ($p < 0.05$). As well, the R^2 was used to evaluate the strength of this linear relationship. For this
 473 process, the resampled and convolved spectra of all samples’ reflectance data were used, and the homologous values
 474 in VNIR bands of MSI and OLI were compared using the 1:1 line. Ideally, these independent variable values should
 475 have a correspondence of 1:1. Additionally, the root mean square difference (RMSD) between both sensors was
 476 derived (Willmott, 1982; Zhang et al., 2018):

$$477 \text{RMSD} = \sqrt{\frac{\sum_i^n (v_i^{OLI} - v_i^{MSI})^2}{n}} \quad (11)$$

479 Where RMSD between corresponding Landsat-OLI and Sentinel-MSI variables values (reflectances and WVI’s), “ v_i ”
 480 is the variable under analysis and “ i ” is the number of variable ($i = 1$ to n).

482 4. Results analysis

483 4.1. Spectral and CRRS analysis

484 Spectral signatures of seagrass and algae species are measured separately and mixed in black and yellow large bowls
 485 using two sedimentary substrates (dark and bright). They are presented separately for the examined coverage rates,
 486 namely 10, 30, 75, and 100% (Fig. 7, a-d). Overall, the reflectance signatures of seagrass and algae samples are similar
 487 to those of healthy vegetation canopy. These reflectance signatures exhibit slight absorption features near 450 nm and
 488 others stronger between 650 and 700 nm with a minimum at 670 nm caused by the chlorophyll; as well as a significant
 489 reflection between 520 and 600 nm due to carotenoid pigments and high reflectance in the NIR attributed to internal
 490 tissue structure (700 to 900 nm). Differently to land vegetation, the red-edge is not well developed (very weak)
 491 particularly for non-dense seagrass and algae due to high red and NIR absorption by water molecules as shown in Fig.
 492 1. Generally, absorption or reflection of pigmentations between species occurs in different wavelengths but the
 493 strength of absorption gradually increases in the red as the coverage rate increases.

494 For scattered and low coverage ($\sim 10\%$), the shapes of all spectra are nearly ~~relatively~~-similar, without the
 495 possibility to identify specific absorption features or to separate among species according to their spectra in the visible
 496 domain (Fig. 7a). The highest reflectance values vary between 10% and 15% across NIR wavelengths with a difference
 497 reflectance ($\Delta\rho_{\text{NIR}}$) around 5%, while in the visible all the reflectance values are below 5% with $\Delta\rho_{\text{visible}}$ are also $< 5\%$.
 498 For this low and sparse cover, it is observed that the reflectance is influenced by spectral properties of the underlying
 499 sediments, fragments of vegetation, light shading, etc., thus contributing to the confusion between spectral signatures.
 500 Definitely, under such conditions, it is a challenge to distinguish between seagrass and/or algae species based only on

501 their spectral signatures. Whereas, the measurements acquired over somewhat denser coverage rates (~ 30 %) show
502 analogous spectral behaviour and patterns with overlap among spectra in visible wavelengths (400 to 700 nm), but a
503 slight separability between species ~~stands out is~~ relatively apparent in NIR (Fig. 7b).

504 Furthermore, unlike scattered or less dense cover ($\leq 30\%$), the analysis of the dense and very dense coverage rates
505 (75 and 100%) showed that the optical properties (darkness or brightness) of the underlying substrate does not have a
506 significant effect on the measured spectra. For these coverage ranges, the clear and normal behaviour of vegetation
507 cover spectra are observed. The absorption feature is weak in the blue (450-480 nm) but more accentuated in red (670
508 nm), the reflection peak is more highlighted in green (550 nm), and the reflectance values increase notably and
509 gradually in NIR with the increase of the coverage rate. Although the seagrass has a distinct spectral response
510 compared to the algae, especially in the green and NIR regions of the spectrum, significant spectral differences are
511 noted for the HU with the highest reflectance, followed by GA, HS, and BA. This order is probably controlled by the
512 leaves structures that are specific for each type of seagrass or algae. The reflectance values in the visible are controlled
513 by the absorption of chlorophyll pigmentations in blue and red wavelengths, and by the carotenoid pigmentations in
514 the green band. In addition, compared to HS and BA spectra, HU and GA showed relatively strong absorption by
515 chlorophyll in red wavelengths. This difference is due to the nature of chlorophyll in each species. Indeed, brown
516 algae contain accessory pigments “fucoxanthin” and chlorophyll “c” (Johnsen and Sakshaug, 2007), while seagrass
517 are flowering plants, and their leaves contain chlorophyll “b” (Cummings and Zimmerman, 2003). It is observed also
518 that the BA carotenoid pigments (fucoxanthin) are characterized by spectral features at 630 and 650 nm that are not
519 present in the spectra of HS, HU, and GA (Fig. 7). However, despite all these spectral characteristics the difference in
520 reflectance values among all species (individual and mixed) is $\leq 6\%$ in the visible and $\leq 13\%$ in NIR for a very dense
521 cover (100%). Therefore, these results suggest that it is probably possible for the blue, green, and NIR wavelengths
522 to discriminate among the considered seagrass and algae species if they are homogeneous with high or very high
523 densities.

524 Otherwise, the CRRS transformations are presented in Fig. 7 (e-h) with Sentinel-MSI relative spectral response
525 profiles characterizing the filters of VNIR bands. The lower CRRS values indicate the greatest potential spectral
526 separability, which means the identification of the appropriate wavelengths to discriminate among the considered
527 classes of investigated species. As shown in Fig. 7 (e-h), the CRRS significantly enhances the spectral separability
528 among the seagrass and algae classes, especially in the visible bands. Two main absorption features are highlighted in
529 the blue (485-498 nm) and red (~ 670 nm) regardless the species. In the green, one major reflection peak is observed
530 around 544 nm for HU and GA, one around 530 nm for HS, and three peaks are well distinguished for BA at 578,
531 595, and 640 nm (Fig. 7h). These differentiation features become clearer as the coverage rates increase especially in
532 blue and NIR wavelengths. For a low coverage rate (~ 10 %), the strongest absorption depth is that of GA (0.46)
533 followed by HU (0.58), HS (0.74), and BA (0.78) in the blue (Fig. 7e). While in the red, CRRS pointed out that
534 regardless of the coverage rate, a strong similarity is observed between HU and GA due to their high content of
535 chlorophyll pigmentation with a depth of absorption around 0.29. ~~Subsequently~~ followed by HS and BA that are
536 characterized by less absorption depth (~ 0.50). In these two waveband domains (blue and red), the absorption features
537 become deeper with increasing coverage density. Likewise, when the cover rate of all species becomes denser (100%),

538 similar absorption characteristics are exhibited in the red band between HU and GA species; as well as between HS
539 and BA (Fig. 7h). While in the blue and NIR wavelengths, the CRRS highlights the distinction and differentiation
540 between species. On the other hand, as the coverage increases from 10 to 100%, the reflection peak in the green
541 waveband becomes less pronounced due to the high content of carotenoid pigment; also a strong similarity is observed
542 between HU and GA. Moreover, the curves of CRRS of the mixed species occupy an intermediate position of
543 absorption features between the homogeneous samples and, therefore, the differentiation between absorption
544 characteristics becomes very ~~narrow~~slight. Accordingly, the discrimination between pure and mixed species becomes
545 very difficult or even impossible. Overall, spectral and CRRS analyses highlighted the importance of the blue, green,
546 and NIR wavelengths for seagrass and algae detection and probable discrimination based on hyperspectral
547 measurements. These results corroborate the physical concept presented in Fig. 1 that the blue and green
548 electromagnetic radiation penetrates a deeper vertical column of water. While despite its limited penetration, the NIR
549 shows a certain sensitivity to the biomass density and its spatial distribution.

550

551

[Figure 7]

552 4.2. Resampling and convolving in OLI and MSI bands

553 Fig. 8 illustrates the scatter-plots between the resampled and convolved reflectance values in the VNIR homologous
554 bands of the MSI and OLI sensors. Simulated at the top of the atmosphere using all considered samples (seawater,
555 sediments, seagrass, algae and mixed species of both seagrass and algae at ~~varied unlike~~ coverage rates), they allow
556 the analysis of the difference in reflectance values ($\Delta\rho$) and RMSD due exclusively to dissimilarities in spectral
557 response function between homologous bands. These scatter-plots reveal a near-perfect fit with 1:1 line expressing an
558 excellent coefficient of determination (R^2 of 0.999) between homologous bands with the slopes and intercepts very
559 near to unity and zero, respectively. Thus, the derived $\Delta\rho$ values are null for VNIR homologous bands for seawater
560 and are insignificant for dark and bright substrate sediments in all bands (i.e., 0.009 for green and 0.002 for the coastal,
561 blue, red, and NIR bands). While, for seagrass and algae (HS, HU, GA, and BA), $\Delta\rho$ vary between 0.003 and 0.02
562 regardless of the coverage rate or the considered spectral band. Moreover, the achieved overall RMSD in reflectance
563 between MSI and OLI homologous bands considering all samples are insignificant (≤ 0.0015) for blue, green, and red
564 bands, and null for coastal and NIR bands. It is also observed that all the bands are insensitive to the variation of the
565 colors of the bowls and the sedimentary substrate optical properties. These results pointed out that MSI and OLI
566 sensors are spectrally similar and can be used jointly for high temporal frequency to monitor seagrass and algae
567 dynamics in time and space. Therefore, due to this near-perfect spectral similarity between these instruments, our
568 analysis in the following sections will focus only on the MSI sensor.

569

570

[Figure 8]

571

572 Fig. 9 illustrates the reflectances of seagrass, algae, and seawater resampled and convolved in VNIR bands of MSI or
573 OLI sensors considering each species separately and all species at different coverage rates. Compared to the measured

574 hyperspectral signatures (Fig. 7), these broadband spectra are more generalized and less precise because these spectra
 575 lost the specific and unique absorption features of seagrass and/or algae species caused by pigmentations as discussed
 576 above. However, such broadband spectra retain the same spectral pattern as the original spectra. Regardless of the
 577 species, the graphics summarized in Fig. 9 exhibit similar shape and pattern, but with a slight difference in reflectance
 578 values between species in the visible bands. If we consider the species separately (HS, HU, GA, and BA) in different
 579 coverage rates (10, 25, 75, and 100%), the reflectance difference values ($\Delta\rho$) are ≤ 0.02 ; and insignificant ($\Delta\rho \leq 0.002$)
 580 for pure seawater and sediments in all VNIR bands. Hence, these species are not spectrally distinguishable particularly
 581 in the visible whatever the coverage. While, if we consider all samples (seagrass, algae, and mixed) in all coverage
 582 rates (Fig. 9e), the $\Delta\rho$ are equal to 0.03 in coastal and blue bands, 0.05 in green, 0.035 in red and 0.21 in NIR. Except
 583 for the NIR, the calculated $\Delta\rho$ values in the visible are approximately identical to the accuracies achieved from
 584 radiometric calibration and atmospheric corrections. Therefore, relying on the multispectral bandwidth of OLI and
 585 MSI sensors, it is difficult or even impossible to differentiate or to map seagrass and algae individually at the species
 586 level. Accordingly, SAV classes' discrimination and mapping will be discussed.

587

588

[Figure 9]

589 4.3. Vegetation indices analysis

590 In this third part, the NDVI, SAVI, EVI, TDVI, NDWI, and DVI indices were implemented and analysed in three
 591 versions each by integrating the red, blue, and green bands; while the indices TGI, VARI, and Diff(G-B) were
 592 calculated and tested respecting their original ~~and unchangeable~~ equations. In total, 21 combinations of indices were
 593 calculated for each sensor. The statistical analyses ($p < 0.05$) focus on the similarity or dissimilarity between MSI and
 594 OLI homologous indices, and their potential for seagrass and algae discrimination. Except for the TGI and VARI
 595 indices, the results revealed an excellent linear relationship (R^2 of 0.999) between MSI and OLI products regardless
 596 of the compared index and the integrated spectral bands (red, green, and blue). Overall, the scatter-plots presented in
 597 Fig. 10 depict a very good fit to the 1:1 line with the slopes and intercepts very near to unity and zero, respectively.
 598 However, despite its near-perfect linearity and insignificant RMSD between MSI and OLI values (0.001), the TGI
 599 show a very weak and limited spatial variability with a range between 0.0 for pure seawater and 0.05 for a very dense
 600 coverage (100%) of seagrass or algae (Fig. 10e). This range cannot allow the differentiation among the marine
 601 environment classes, because this index was not developed for biomass sensing but was designed for crop nitrogen
 602 requirements detection. Likewise, although the scatter-plot of VARI shows an excellent coefficient of determination
 603 (R^2 of 0.99), this index ~~estimates with the overestimates the predicted values by~~ MSI sensor ~~exceed compared to~~ those
 604 estimated ~~from by~~ OLI, resulting in the data not fitting the 1:1 line very well (Fig. 10f). Moreover, the difference
 605 values of VARI derived from MSI and OLI data vary between 0.0 and 0.14 depending on the sample species and its
 606 coverage rate, with an overall RMSD of 0.03. This result can be explained by the fact that the VARI uses only the
 607 visible ranges of the spectrum and does not consider the NIR band, which is the most informative about the biomass
 608 density. In addition, it was developed particularly for very dense (100%) wheat crops; moreover, it was designed
 609 principally for coarse data acquired by the SeaWiFS, MODIS, MISR, and MERIS sensors. According to Gitelson et

610 al. (2002b), many factors potentially decrease the accuracy of the VARI ~~such as vegetation (e.g. vegetation cover~~
 611 ~~species, canopy architecture, and sun illumination geometry)~~. For wheat and corn species, this index yielded RMSE
 612 of around 10% (Gitelson et al., 2002a). Therefore, the weaknesses raised for these two indices (TGI and VARI) are
 613 not caused by the impact due exclusively to the dissimilarities in spectral response function between homologous
 614 bands of MSI and OLI sensors, but due to their mathematical concepts that are intended for a single and specific
 615 application.

616 Furthermore, the scatter-plots presented in Fig. 10 (a-d) are showing examples of certain indices including NDWI,
 617 WAVI, WEVI, and WTDVI. Overall, the indices are fitting very well the 1:1 line with R^2 of 0.99, slopes very near to
 618 unity and intercepts to zero. The indices show that the derived WVI from MSI and OLI data ~~are predicting similarly~~
 619 ~~give similar estimates of~~ seagrass and algae species in a shallow marine environment. Considering all investigated
 620 samples in this study, the interval difference values between homologous indices vary between 0.0 and 0.01 for all
 621 versions of WTDVI, WAVI, WDVI, and Diff(G-B); while they vary between 0.0 and 0.04 for NDWI, WEVI and
 622 NDWI. These differences values are satisfactory and remain equal to or less than the combined inaccuracies of
 623 atmospheric corrections and sensor radiometric calibration. Moreover, the achieved RMSD values between MSI and
 624 OLI homologous indices are insignificant ($RMSD \leq 0.01$) for all indices (Table 2) regardless of the integrated spectral
 625 band. These analyses pointed out that MSI and OLI sensors can be combined for high temporal frequency to monitor
 626 the dynamic of biophysical products in time and space in a shallow marine environment.

627

628 [Table 2]

629

630 [Figure 10]

631

632 Fig. 11 summarises the linear regressions ($p < 0.05$) between the best indices and the reflectances in NIR considering
 633 all samples, i.e., seawater, sediments, seagrass, algae, and mixed species classes with different coverage rates (10, 30,
 634 75, and 100%). The computed indices (NDVI, SAVI, EVI, TDVI, NDWI, and DVI) with the blue, green, and red
 635 bands are the most relevant for SAV differentiation and mapping. Firstly, it is observed that the indices NDVI and
 636 NDWI provided similar results with opposite signs, i.e., symmetrically opposed concerning the X-axis. Indeed,
 637 whatever the integrated band, the NDWI results are always symmetrical compared to those of NDVI but with negative
 638 values. However, such results are not showing the truth because negative values are automatically reset to zero by the
 639 image processing system and, therefore, it is probable that the results will be inaccurate. Furthermore, when the red
 640 and blue bands are implemented in the NDVI equation, insignificant fits (R^2 of 0.40) were achieved. ~~While, ; but~~
 641 improved results are obtained with the integration of the green band (R^2 of 0.63) and the index is named NDWVI.
 642 Analogous results are obtained by Diff(G-B) and VARI indices with R^2 of 0.63 (Table 2) when all samples are
 643 considered. Luckily, the statistical fits of these three indices (NDWVI, Diff(G-B), and VARI) becomes significantly
 644 improved when unique species is considered, such as only seagrass or only algae (R^2 of 0.85). Whereas, in addition
 645 to its weakness and limited sensitivity to the spatial variability of seagrass and algae, the TGI was irrelevant for SAV
 646 discrimination yielding a very low fits (R^2 of 0.20) whatever the considered species.

647
648 [Figure 11]
649
650 As discussed previously, when integrating the blue and green bands, the indices WdVI, WdAVI, WEVI, and
651 WTDVI outperformed all examined indices regardless of the species (seagrass, algae, or mixed), yielding a very
652 significant coefficient of determination for mixed species ($0.89 \leq R^2 \leq 0.96$) (Fig. 11 a-d, and Table 2). Calculated
653 with blue, green, or red bands, the DVI (noted WdVI) discriminated among SAV classes significantly ($R^2 \leq 0.92$),
654 but it underestimates the SAV as shown in Fig. 10-d. However, WdAVI, WEVI, and WTDVI offer similar trends
655 regardless the considered species ($R^2 \leq 0.92$ for mixed or seagrass only, and R^2 of 0.82 for algae only). Overall, instead
656 of the red band, the integration of blue and green bands in vegetation indices increases their discriminating power for
657 SAV (Table 2). These results corroborate the spectral analysis and the CRRS transformations; the blue and green
658 electromagnetic radiation penetrates deeper through the water allowing more details and information about marine
659 vegetation discrimination. This finding is consistent with Wicaksono and Hafizt (2013), and Villa et al. (2014) where
660 the blue band better separates and maps aquatic vegetation features over some lake ecosystems in Italy. However, the
661 summarized R^2 in Table 2 shows that the indices WdAVI, WEVI, and WTDVI provided ~~relatively identical~~ very close
662 results when integrating the blue or green bands. Nevertheless, the scatter plots in Fig. 11 (a, b, and c) illustrate that
663 when the green band is considered instead of the blue, the majority of sampled points are located closer to line 1:1,
664 especially when the coverage rate becomes denser. This can be explained by the fact that despite the power of blue
665 wavelengths to penetrate deeper into the water, this band also leads to an overestimation of indices values due to its
666 higher scattering (Fig. 11), mainly in turbid environments.

667 5. Discussion

668 Seagrass and algae species showed similar spectral signature curves, but with subtle differences between species. In
669 general, some relevant wavelengths are observed for the characterization of the considered species of seagrass and
670 algae including those at or near 450, 500, 520, 550, 600, 620, 640, 670, and 700 nm. They are related to the absorption
671 features and reflection peaks due to photosynthetic pigmentations of HU, HS, GA, and BA. Spectral and CRRS
672 analyses highlighted the importance of the blue, green, and NIR wavelengths for probable differentiation between the
673 considered seagrass and algae types. However, the magnitude of the $\Delta\rho$ values among species is an indicator of the
674 strength of the absorption feature depths and, therefore, of their discriminating power between species. For instance,
675 the highest $\Delta\rho$ values among all considered samples (seagrass, algae, and mixed of both) is $\leq 5\%$ across the visible
676 wavelengths and around 10 to 15% in NIR. Likewise, the CRRS transformations of all spectra of homogeneous and
677 mixed samples show that the absorption characteristics become all very similar and, thus, the discrimination between
678 pure and mixed species becomes difficult or even impossible. These results are in agreement with other findings that
679 have been conducted in many geographic locations worldwide and have considered many seagrass and algae types.
680 Considering nine tropical species of seagrass, Wicaksono et al. (2019) showed that even hyperspectral data will not
681 improve discrimination between seagrass and algae at the species level in pixels or sub-pixels due to the subtle
682 difference in absorption features among them. As well, Phinn *et al.* (2008) confirmed that the hyperspectral data are

683 unable to map seagrass biomass at the species level in shallow waters of Moreton Bay in Australia. Using field and
684 laboratory hyperspectral measurements over several seagrass species on the west coast of Florida, Pu et al. (2012)
685 reported also that the VNIR wavelengths have relatively low accuracies to discriminate among seagrass community
686 composition.

687 Otherwise, the resampled and convolved spectra in VNIR bands of MSI and OLI sensors are similar in all cases,
688 considering each species separately or the totality of samples at different coverage rates. These spectra are more
689 generalized and less precise due to the loss of absorption features caused by pigmentations. Hence, regardless of the
690 coverage rates, if uniform and homogeneous ~~ize~~-species are considered, the $\Delta\rho$ is ≤ 0.02 in the visible and is ≤ 0.22
691 in NIR. While, if all mixed samples and species are considered at the investigated coverage rates, $\Delta\rho$ is ≤ 0.05 in
692 visible bands and remains stable ($\Delta\rho \leq 0.22$) in NIR. These very small values do not allow spectral distinction among
693 species, particularly in the visible wavebands. Therefore, based on the multispectral bandwidth of OLI and MSI
694 sensors, it is difficult to differentiate seagrass and algae individually at the species level. Indeed, it is important to
695 remember that these simulations were conducted in a Goniometric-Laboratory using close range measurements
696 protocol and supervising rigorously all measured samples, i.e., homogeneous, or mixed. Moreover, in this controlled
697 environment, the atmospheric scattering and absorption are absent; errors related to the sensor radiometric calibration
698 are also absent, no wave's variation, no residual clouds contamination, no sun-glint (specular effects), no variability
699 in water depth, and no BRDF impact. However, the results obtained are not entirely conclusive and do not provide a
700 clear and satisfactory distinction among the spectral signatures of the investigated species. The difference among
701 spectral signatures is surely reduced in the real world when seagrasses and algae are embedded in sediments and
702 overlaid by water column and constituents including phytoplankton, suspended organic and inorganic matter,
703 variability in water depth, and remote sensing problems (internal and external). Additionally, the acquired images with
704 Sentinel-MSI (2A and 2B) and Landsat-OLI (8 and 9) sensors are coded radiometrically in 12 and 16 bits, respectively.
705 These images cover dissimilar pixels surfaces of 100 m² for MSI and 900 m² for OLI, where SAV information can be
706 easily mixed within pixels. Besides, the FOV of these instruments are different, OLI's FOV is 15° covering a swath
707 of 185 km, while the MSI is characterized by a large FOV of 20.6° covering a swath of 290 km, which requires the
708 adjustments to reduce differences caused by BRDF effects (acquisition and sun illumination geometries). Data quality
709 may also change due to the sensor's radiometric performance, SNR, and atmospheric interferences (diffusion and
710 absorption). ~~Nevertheless, despite~~ Despite the corrections of all these anomalies before the information extraction,
711 biases still occur generated by errors propagation, which affect the recorded signal at the sensor level and, therefore,
712 the precision of discrimination between seagrass and algae at the species level. For instance, if we consider the
713 published RMSE regarding each source of error separately, the calculated total RMSE based on errors propagation
714 theory (equation 12) will be approximately 0.08 to 0.10 (reflectance unit). Therefore, this total RMSE is greater than
715 the achieved difference between reflectance values ($\Delta\rho \leq 0.05$), especially in the visible bands. Accordingly, it is
716 impossible to differentiate between seagrass and algae at the species level. Likewise, this total RMSE is solely due to
717 the limitations of remote sensing methods, but it can also be amplified by environmental ~~restrictions~~ aspects of
718 seagrass habitat, as discussed above and reported by Wicaksono and Hafizt (2013).

719

$$720 \quad \text{RMSE}_{\text{Total}} = [(\sigma_{\text{Sensor-drift}})^2 + (\sigma_{\text{Atmosphere}})^2 + (\sigma_{\text{Sun-glnt}})^2 + (\sigma_{\text{BRDF}})^2 + (\sigma_{\text{Water-column}})^2]^{0.5} \quad (12)$$

721

722 Where:

723 $\sigma_{\text{Sensor-drift}}$: Sensor radiometric calibration accuracy, ± 0.03 (Markhman et al., 2014 and 2016),724 $\sigma_{\text{Atmosphere}}$: Atmospheric corrections accuracy, mostly around ± 0.03 to ± 0.05 in the visible bands (Vermote et al.,
725 2016),726 $\sigma_{\text{Sun-glnt}}$: Sun glint correction accuracy, ± 0.05 (Zorrilla et al., 2019),727 σ_{BRDF} : Accuracy of BRDF correction for MSI, ± 0.05 to ± 0.08 (Roy et al., 2017),728 $\sigma_{\text{Water-column}}$: Accuracy of water column correction, ± 0.04 (Zoffoli et al., 2014).

729

730 The results of this research accomplished in the Arabian Gulf species based on spectroradiometric measurements are
731 consistent with other researches carried out in many geographical regions worldwide. Barillé et al. (2009) showed the
732 degradation of spectral features when resampled into SPOT-HRV visible bands and, therefore, seagrass species could
733 no longer be discriminated in these wavelengths. This statement is also in agreement with Wicaksono et al. (2017)
734 who reported that resampled spectra in MSI and OLI bands do not have sufficient spectral information for seagrass
735 species discrimination for accurate classification. Using MSI and OLI data with respectively 10 m and 30 m pixel
736 sizes (i.e., each OLI pixel is represented by 9 MSI pixels), Lyons et al. (2011) reported relatively accurate
737 discrimination between seagrass meadows spots that are very large with homogenous composition and distinct
738 boundaries between species. While, the differentiation becomes impossible when the analyzed spots are composed of
739 diverse species and scattered without clear boundary.

740 Furthermore, to analyze the impact of differences in reflectance exclusively due to dissimilarities in spectral
741 response function between homologous spectral bands, the scatter-plots between SMI and OLI simulated surface
742 reflectance values at the top of the atmosphere revealed a very good linear relationship (R^2 of 0.999) between VNIR
743 homologous bands. The slopes and intercepts are nearly equal to unity and zero, respectively. It is also observed that
744 independently to the sediments substrate (dark and bright) or the color of used bowls (black or yellow), the $\Delta\rho$ values
745 between VNIR homologous bands vary in the range of 0.003 to 0.02, regardless of the observed species (seagrass,
746 algae and mixed) or the coverage rate. Moreover, the achieved overall RMSD in reflectance values are very small (\leq
747 0.0015) for all VNIR bands, i.e., smaller than the uncertainty of the radiometric calibration process (0.03) as
748 demonstrated by Markham et al. (2016). In other respect, all the derived homologous WVI values fit near-perfectly
749 with the 1:1 line expressing an excellent coefficient of determination (R^2 of 0.99), a slope of 0.99 and intercept equal
750 to zero. Moreover, the achieved RMSD values between MSI and OLI homologous indices are insignificant ($\text{RMSD} \leq$
751 0.01) for all indices regardless of the integrated spectral band (red, green, and blue). These results corroborate the
752 finding of Wicaksono et al. (2019) who reported that MSI and OLI had similar results for tropical seagrass species
753 analysis using simulated reflectance spectra and imagery data. Moreover, using simulated data and images acquired
754 simultaneously with MSI and OLI over a wide variety of land cover types including open shallow water, Mandanici
755 and Bitelli (2016) showed a very high coefficient of determination (R^2 of 0.98) between homologous bands. Therefore,
756 these results pointed out that the examined sensors, MSI onboard Sentinel-2A/2B and OLI onboard Landsat-8/9, can

757 be combined for the marine environment and SAV detection, mapping, and monitoring during shorter time intervals
758 or for consecutive observations. However, rigorous pre-processing issues (sensors calibration, atmospheric
759 corrections, sun-glint corrections, and BRDF normalization) must be addressed before the joint use of acquired data
760 with these sensors. Furthermore, we demonstrated that blue and green bands are better than red for seagrass and algae
761 biomass discrimination, providing the best R^2 and the most insignificant RMSD for the investigated indices. Green
762 rather than the blue band integration is preferable due to its better sensitivity to pigment content within seagrass and
763 algae tissues, for its ability to penetrate water, and for its low sensibility to atmosphere and water column scattering.

764 6. Conclusions

765 The MSI sensors onboard Sentinel satellites 2A/2B and the OLI instruments installed on Landsat 8/9 satellites are
766 designed to be similar in the perspective that their data be used together to support global Earth surface reflectances
767 coverage for science and development applications at medium spatial resolution and near-daily temporal resolution.
768 However, relative spectral response profiles characterizing the filter's responsivities of these instruments are not
769 identical between the homologous bands, so some differences are probably expected in the recorded shallow water
770 reflectance values for seagrass, algae, and mixed species differentiation and mapping. Based on spectral analysis and
771 CRRS transformation, the results of the present research pointed out subtle spectral differences between seagrass (HU
772 and HS), algae (green and brown), or mixed species, particularly in the blue, green, and NIR wavelengths. However,
773 once resampled and convolved in MSI and OLI homologous VNIR bands, similar patterns to the original spectra are
774 observed but with severe generalisation and loss of specific absorption features. Therefore, mapping seagrass and/or
775 algae at the species level in shallow marine waters is a very difficult if not impossible task, either using multispectral
776 bandwidth of MSI and OLI sensors or even hyperspectral data. Moreover, different from these ideal simulations in a
777 controlled environment, the mapping would be more difficult in a real marine habitat where various species are mixed
778 and interleaved with each other, as well as the propagation of internal and external errors related to remote sensing
779 data. Hence, it is recommended to discuss SAV rather than ~~the~~ mapping seagrass or algae at the species level.

780 Furthermore, instead of the red band, the integration of the blue and green bands in WVI increases their
781 discriminating power and ability ~~to -of map~~ SAV, particularly WAVI, WEVI, and WTDVI indices. These results
782 corroborate the spectral analysis and the CRRS transformations showing that the blue and green electromagnetic
783 radiation allows better marine vegetation differentiation. Nevertheless, despite the power of blue wavelength to
784 penetrate deeper into the water, it also leads to a relative overestimation of dense SAV coverage due to the higher
785 scattering in this part of the spectrum, particularly in the turbid environment. Furthermore, statistical fits between SMI
786 and OLI simulated surface reflectance over the considered samples reveal an excellent linear relationship (R^2 of 0.999)
787 between all homologous VNIR bands. The achieved RMSD values are extremely small between the NIR homologous
788 bands and insignificant for the other bands (≤ 0.0015). Moreover, independently of the analysed samples,
789 homogeneous (seagrass or algae) or mixed (seagrass plus algae), good agreements ($0.63 \leq R^2 \leq 0.96$) were also
790 obtained between homologous WVI regardless of the integrated spectral bands (i.e., red, green, and blue), yielding
791 insignificant RMSD (≤ 0.01). These achieved RMSD values for reflectances or WVI's are less than the combined
792 errors related to sensor radiometric calibration and atmospheric corrections. Accordingly, these results pointed out

793 that MSI and OLI sensors are spectrally similar and can be combined for high temporal frequency to monitor
794 accurately the SAV and its dynamic distribution in time and space in the shallow marine environment. However,
795 rigorous pre-processing issues such as sensors calibration, atmospheric corrections, BRDF normalisation, sun glint,
796 and water column corrections must be addressed before the joint use of acquired data with these sensors.

797

798 **7. Data Availability:** The authors confirm that the data supporting the findings of this study are available.

799

800 **87. Author Contributions:** Professor A. Bannari performed the paper conceptualization, field data collection, pre-
801 processing and processing, results analyses and paper writing. Professor S.T. Ali assisted in the field sampling, the
802 results analyses and the paper writing. Professor A. Abuhussain assisted in the results interpretation, analyses and
803 paper writing. All authors have read and agreed to the published version of the manuscript.

804

805 **98. Competing Interests:** The authors declare no conflict of interest.

806

807 **109. Acknowledgements**

808 The authors would like to thank the Arabian Gulf University (Kingdom of Bahrain) for the financial support for the
809 field data collection, and to Marine and Environment Arabia Consultancy Services (Manama, Bahrain), for providing
810 photographs and making them available for consultation and public use. Our gratitude goes also to the anonymous
811 reviewers for their constructive comments.

812

813 **110. References**

814 Anders, K. and Lina, N.: Remote sensing of seagrasses in a patchy multi-species environment. *International Journal*
815 *of Remote Sensing*, 32(8), 2227 – 2244, 2011.

816 ASD: Analytical Spectral Devices. Technical Guide, 4th ed.; ASD Inc.: Boulder, CO, USA. Available online:
817 <http://www.asdi.com/products-spectroradiometers.asp> (accessed on 30 September 2020), 2015.

818 Bakirman, T. and Gumusay, M. U.: Assessment of Machine Learning Methods for Seagrass Classification in the
819 Mediterranean. *Baltic J. Modern Computing*, 8(2), 315-326. <https://doi.org/10.22364/bjmc.2020.8.2.07> , 2020.

820 Bannari, A.: Synergy between Sentinel-MSI and Landsat-OLI to Support High Temporal Frequency for Soil Salinity
821 Monitoring in an Arid Landscape. In: *Research Developments in Saline Agriculture*, edited by Jagdish Chander
822 Dagar, Rajender Kumar Yadav, and Parbodh Chander Sharma. Published by Springer Nature Singapore Pte Ltd.,
823 pp. 67-93, ISBN: 978-981-13-5831-9. https://doi.org/10.1007/978-981-13-5832-6_3, 2019.

824 Bannari, A., Morin, D., Huete, A. R. and Bonn, F.: A Review of Vegetation indices. *Remote Sensing Reviews*, 13,
825 95-120, 1995.

826 Bannari, A., Asalhi, H. and Teillet, P. M.: Transformed Difference Vegetation Index (TDVI) for Vegetation cover
827 Mapping. *International Geoscience and Remote Sensing Symposium (IGARSS'2002)*, Toronto, Ontario, 9-13
828 July, pp. 3053-3055, 2002.

- 829 Bannari, A., Teillet, P. M., and Landry, R.: Comparaison des réflectances des surfaces naturelles dans les bandes
830 spectrales homologues des capteurs TM de Landsat-5 et TME+ de Landsat-7. *Revue Télédétection*, 4(3), 263-275,
831 2004.
- 832 Bannari, A. and Kadhem, G.: MBES-CARIS Data Validation for Bathymetric Mapping of Shallow Water in the
833 Kingdom of Bahrain on the Arabian Gulf. *Remote Sensing*, 9, 385-404, 2017.
- 834 Bannari, A. and Al-Ali, Z.: Ground Reflectance Factor Retrieval from Landsat (MSS, TM, ETM+, and OLI) Time
835 Series Data based on Semi-empirical Line Approach and Pseudo-invariant Targets in Arid Landscape.
836 International Geoscience and Remote Sensing Symposium (IGARSS-2020), July 19-24th, Waikoloa, Hawaii,
837 USA, pp. 5990-5993, 2020.
- 838 Barillé, L., Mouget, J. L., Méléder, V., Rosa, P., Jesus, B.: Spectral response of benthic diatoms with different
839 sediment backgrounds. *Remote Sensing of Environment*, 115(4), 1034–1042, 2011.
- 840 Barillé, L., Robin, M., Harin, N., Bargain, A. and Launeau, P.: Increase in seagrass distribution at Bourgneuf Bay
841 (France) detected by spatial remote sensing. *Aquatic Botany*, 92(3), 185-194, 2010.
- 842 Bargain, A., Robin, M., Le-Men, E., Huete, A. R. and Barillé, L.: Spectral response of the seagrass *Zostera noltii* with
843 different sediment backgrounds. *Aquatic Botany*, 98, 45-56, 2012.
- 844 Bayyana, S., Pawar, S., Gole, S., Dudhat, S., Pande, A., Mitra, D., Johnson, J. A. and Sivakumar, K.: Detection and
845 mapping of seagrass meadows at Ritchie's archipelago using Sentinel 2A satellite imagery. *Current Science*,
846 118(8), 1275-1282. DOI: 10.18520/cs/v118/i8/1275-1282, 2020.
- 847 Ben-Dor, E., Ong, C. and Lau, I. C.: Reflectance measurements of soils in the laboratory: Standards and protocols.
848 *Geoderma*, 245–246, 112–124, 2015.
- 849 Boström, C., Pittman, S., Kneib, R. and Simenstad, C.: Seascape ecology of coastal biogenic habitats: advances, gaps
850 and challenges. *Marine Ecology Progress Series*, 427, 191– 217, 2011.
- 851 Burfeind, D. D. and Stunz, G. W.: The effects of boat propeller scarring intensity on nekton abundance in subtropical
852 seagrass meadows. *Marine Biology (Berlin)*, 148, 953–962, 2006.
- 853 Candra, E. D., Hartono, and Wicaksono, P.: Above Ground Carbon Stock Estimates of Mangrove Forest Using
854 Worldview-2 Imagery in Teluk Bena, Bali. *IOP Conference Series: Earth and Environmental Science*, 47(1).
855 <https://doi.org/10.1088/1755-1315/47/1/012014>, 2016.
- 856 Chen, C.-F., Lau, A.-K., Chang, N.-B., Son, N.-T., Tong, P.-H.-S and Chiang, S.-H.: Multi-temporal change detection
857 of seagrass beds using integrated Landsat TM/ETM+/OLI imageries in Cam Ranh Bay, Vietnam. *Ecological*
858 *Informatics*, 35, 43-54, 2016.
- 859 Clark, R. N. and Roush, T. L.: Reflectance spectroscopy: Quantitative analysis techniques for remote sensing
860 applications. *Journal of Geophysical Research*, 89, 6329–6340, 1984.
- 861 Clark, R. N., King, T. V. V. and Gorelick, N. S.: Automatic continuum analysis of reflectance spectra. In JPL
862 Proceedings of the 3rd Airborne Imaging Spectrometer Data Analysis Workshop, 138-142. Available on line:
863 <https://ntrs.nasa.gov/archive/nasa/casi.ntrs.nasa.gov/19880004388.pdf> (accessed on 18 March 2021), 1987.
- 864 Clark, R. N., Gallagher, A. J. and Swayze, G. A.: Material absorption-band depth mapping of imaging spectrometer
865 data using the complete band shape least-squares algorithm simultaneously fit to multiple spectral features from

- 866 multiple materials. In: Proceedings of the Third Airborne Visible/Infrared Imaging Spectrometer (AVIRIS)
867 Workshop, NASA - Jet Propulsion Laboratory Publications, No. 90-54, pp. 176–186, 1990.
- 868 Clark, R. N. and Swayze, G. A.: Mapping minerals, amorphous materials, environmental materials, vegetation, water,
869 ice and snow, and other materials. The USGS Tricorder algorithm, *in* Green, R.O., ed., Summaries of the fifth
870 annual NASA Jet Propulsion Laboratory airborne earth science workshop: Pasadena, NASA Jet Propulsion
871 Laboratory Publication, 95(1), 39-40, 1995.
- 872 Clark, R. N., Swayze, G. A., Carlson, R., Grundy, W. and Noll, K.: Spectroscopy from Space. *Reviews in Mineralogy*
873 *and Geochemistry*, 78(1), 399-446. DOI:10.2138/rmg.2014.78.10, 2014.
- 874 Crowley, J. K., Brickey, D. W. and Rowan, L. C.: Airborne imaging spectrometer data of the Ruby Mountains,
875 Montana: mineral discrimination using relative absorption band-depth images. *Remote Sensing of Environment*,
876 29(2), 121–134. [https://doi.org/10.1016/0034-4257\(89\)90021-7](https://doi.org/10.1016/0034-4257(89)90021-7), 1989.
- 877 Cummings, M. E. and Zimmerman, R. C.: Light harvesting and the package effect in the seagrasses *Thalassia*
878 *testudinum* Banks ex König and *Zostera marina* L.: Optical constraints on photo-acclimation. *Aquatic Botany*, 75,
879 261–274, 2003.
- 880 Dahdouh-Guebas, F., Coppejans, E. and Van-Speybroeck, D.: Remote sensing and zonation of seagrasses and algae
881 along the Kenyan coast. *Hydrobiologia*, 400, 63-73, 1999.
- 882 Dattola, L., Rende, S. F., Dominici, R., Lanera, P., Di-Mento, R., Scalise, S., Cappa, P., Oranges, T. and Aramini, G.:
883 Comparison of Sentinel-2 and Landsat-8 OLI satellite images vs. high spatial resolution images (MIVIS and
884 WorldView-2) for mapping *Posidonia oceanica* meadows. Proceedings of SPIE 10784, Remote Sensing of the
885 Ocean, Sea Ice, Coastal Waters, and Large Water Regions, 10 October 2018, Vol. 10784, 1078419-1; doi:
886 10.1117/12.2326798, 2018.
- 887 Davranche, A., Lefebvre, G. and Poulin, B.: Wetland monitoring using classification trees and SPOT-5 seasonal time
888 series. *Remote Sensing of Environment*, 114(3), 552–562, 2010.
- 889 Dean, A. and Salim, A.: Remote sensing for the sustainable development of offshore mariculture. In: *A global*
890 *assessment of offshore mariculture potential from a spatial perspective*, edited by: Kapetsky, J. M., Aguilar-
891 Manjarrez, J. and Jenness, J.: FAO Fisheries and Aquaculture Technical Paper N. 549, Rome, Italy, 181 pp, 2013.
- 892 Dekker, A. G., Hestir, E. L., Malthus, T. J. and Thankappan, M.: Continental Scale Aquatic Habitat Monitoring Using
893 Sentinel-2. ESA-ESRIN, Frascati, Italy, 23 to 27 April; 28 pp, 2012
- 894 Den-Hartog, C.: The seagrasses of the world. North-Holland Publishing Company, Amsterdam, Netherland, 275 pp.
895 <https://doi.org/10.1002/iroh.19710560139>, 1970.
- 896 Dierssen, H. M., Chlus, A. and Russell, B.: Hyperspectral discrimination of floating mats of seagrass wrack and the
897 macroalgae *Sargassum* in coastal waters of Greater Florida Bay using airborne remote sensing. *Remote Sensing*
898 *of Environment*, 167, 247-258, 2015.
- 899 Drusch, M., Del-Bello, U., Carlier, S., Colin, O., Fernandez, V., Gascon, F., Hoersch, B., Isola, C. Laberinti, P.,
900 Martimort, P., Meygret, A., Spoto, F., Sy, O., Marchese, F., Bargellini, P.: Sentinel-2: ESA's optical high-
901 resolution mission for GMES operational services. *Remote Sensing of Environment*, 120, 25–36.
902 <https://doi.org/10.1016/j.rse.2011.11.026>, 2012.

- 903 Duarte, C. M. and Gattuso, J.-P.: Seagrass meadows. In Encyclopedia of Earth. Edited by Cutler J. Cleveland;
904 Environmental information coalition National Council for Science and the Environment, Washington, DC, USA,
905 2008.
- 906 Duarte, C. M., Losada, I. J., Hendriks, I. E., Mazarrasa, I. and Marbà, N.: The role of coastal plant communities for
907 climate change mitigation and adaptation. *Nature Climate Change*, 3(11), 961–968.
908 <https://doi.org/10.1038/nclimate1970>, 2013.
- 909 Duffy, J. P., Pratt, L., Anderson, K., Land, P. E. and Shutler, J. D.: Spatial assessment of intertidal seagrass meadows
910 using optical imaging systems and a lightweight drone. *Estuarine, Coastal and Shelf Science*, 200, 169–180, 2018.
- 911 Dunton, K. H., and Schonberg, S. V.: Assessment of propeller scarring in seagrass beds of the south Texas coast:
912 *Journal Coastal Research*, 37, 100–110, 2002.
- 913 ENVI: Continuum Removal Tutorial. Boulder, Colorado, USA.
914 <http://www.harrisgeospatial.com/docs/ContinuumRemoval.html> , 2017.
- 915 Erftemeijer, P. L. A. and Shuail, D. A.: Seagrass Habitats in Arabian Gulf: Distribution, Tolerance Thresholds and
916 Threats. *Aquatic Ecosystem Health and Management*, 15(1), 73-83, 2012.
- 917 Ferguson, R. L. and Wood, L. L.: Mapping Submerged Aquatic Vegetation in North Carolina with Conventional
918 Aerial Photography. Federal Coastal Wetland Mapping Programs, National Ocean Pollution Policy Board's
919 Habitat Loss and Modification Working Group. Biological Report, 90(18), pp. 125 – 132. Also available in web:
920 <https://apps.dtic.mil/sti/pdfs/ADA322827.pdf#page=123>, 1990.
- 921 Flood, N.: Comparing Sentinel-2A and Landsat 7 and 8 Using Surface Reflectance over Australia. *Remote Sensing*,
922 9, 659, 2017. DOI: 10.3390/rs9070659, 2017.
- 923 Fourqurean, J. W., Duarte, C. M., Kennedy, H., Marbà, N., Holmer, M., Mateo, M. A., Apostolaki, E. T., Kendrick,
924 G. A., Krause-Jensen, D., McGlathery, K. D. and Serrano, O.: Seagrass ecosystems as a globally significant carbon
925 stock. *Nature Geoscience*, 5(7), 505–509, 2012.
- 926 Fyfe, S. K.: Spatial and temporal variation in spectral reflectance: Are seagrass species spectrally distinct? *Limnology*
927 *and Oceanography*, 48(1, part 2), 464–479. http://dx.doi.org/10.4319/lo.2003.48.1_part_2.0464, 2003.
- 928 Gascon, F., Bouzinac, C., Thépaut, O., Jung, M., Francesconi, B., Louis, J., Lonjou, V., Lafrance, B., Massera, S.,
929 Gaudel-Vacaresse, A., Languille, F., Alhammoud, B., Viallefont, F., Pflug, B., Bieniarz, J., Clerc, S., Pessiot, L.,
930 Trémas, T., Cadau, E., De Bonis, R., Isola, C., Martimort, P. and Fernandez, V.: Copernicus Sentinel-2A
931 Calibration and Products Validation Status. *Remote Sensing*, 9, 584. <https://doi.org/10.3390/rs9060584>, 2017.
- 932 Gitelson, A. A., Kaufman, Y. J., Stark, R. and Rundquist, D.: Novel algorithms for remote estimation of vegetation
933 fraction. *Remote Sensing of Environment*, 80, 76–87, 2002a.
- 934 Gitelson, A. A., Stark, R., Grits, U., Rundquist, D., Kaufman, Y. J. and Derry, D.: Vegetation and soil lines in visible
935 spectral space: a concept and technique for remote estimation of vegetation fraction. *Int. Journal of Remote*
936 *Sensing*, 23(13), 2537–2562, 2002b.
- 937 Green, E. P. and Short, F.: World atlas of seagrasses. Prepared by the UIMEP World Conservation Monitoring Centre.
938 University of California Press, Berkeley, USA, Volume 47. Berkeley (California, USA): University of California.
939 <https://doi.org/10.1515/BOT.2004.029>, 2003.

- 940 Grech, A., Chartrand-Miller, K., Erfemeijer, P., Fonseca, M., McKenzie, L., Rasheed, M. and Coles, R.: A
941 comparison of threats, vulnerabilities and management approaches in global seagrass bioregions. *Environmental*
942 *Research Letters*, 7(2), 024006, 2012.
- 943 Hamel, M. A. and Andréfouët, S.: Using very high resolution remote sensing for the management of coral reef
944 fisheries: review and perspectives. *Marine Pollution Bulletin*, 60(9),1397-405. DOI:
945 10.1016/j.marpolbul.2010.07.002. Epub 2010 Jul 24, 2010.
- 946 Hashim, M., Misbari, S., Yahya, N. N., Ahmad, S., Reba, M. N. and Komatsu, T.: An approach for quantification of
947 submerged seagrass biomass in shallow turbid coastal waters. In *Proceedings of IGARSS, Quebec, Canada*, pp.
948 4439-4442. DOI: 10.1109/IGARSS.2014.6947476, 2014.
- 949 Hedley, J., Roelfsema, C., Koetz, B. and Phinn, S.: Capability of the Sentinel 2 mission for tropical coral reef mapping
950 and coral bleaching detection. *Remote Sensing of Environment*, 120, 145–155, 2012a.
- 951 Hedley, J. D., Roelfsema, C. M., Phinn, S. R. and Mumby, P. J.: Environmental and sensor limitations in optical
952 remote sensing of coral reefs: implications for monitoring and sensor design. *Remote Sensing*, 4, 271-302.
953 <http://dx.doi.org/10.3390/rs4010271>, 2012b.
- 954 Hossain, M. S., Bujang, J. S., Zakaria, M. H. and Hashim, M.: The application of remote sensing to seagrass
955 ecosystems: An overview and future research prospects. *Int. J. Remote Sensing*, 36(1), 61–113, 2014.
- 956 Huang, Z., Turner, B. J., Dury, S. J., Wallis, I. R. and Foley, W. J.: Estimating foliage nitrogen concentration from
957 HYMAP data using continuum removal analysis. *Remote Sensing of Environment*, 93, 18–29, 2004.
- 958 Huete, A. R.: A soil-adjusted vegetation index (SAVI). *Remote Sensing of Environment*, 25, 295-309, 1988.
- 959 Huete, A. R., Didan, K., Miura, T., Rodriguez, E. P., Gao, X. and Ferreira, L. G.: Overview of the radiometric and
960 biophysical performance of the MODIS vegetation indices. *Remote Sensing of Environment*, 83(1), 195-213.
961 [http://dx.doi.org/10.1016/S0034-4257\(02\)00096-2](http://dx.doi.org/10.1016/S0034-4257(02)00096-2), 2002.
- 962 Hunt, Jr. E. R., Doraiswamy, P. C., McMurtrey, J. E., Daughtry, C. S. T., Perry, E. M., and Akhmedov, B.: A visible
963 band index for remote sensing leaf chlorophyll content at the canopy scale. *Int. Journal of Applied Earth*
964 *Observation and Geoinformation*, 21, 103–112, 2013.
- 965 Indayani, A. B., Danoedoro, P., Wicaksono, P., Winarso, G. and Setiawan, K. T.: Spectral Analysis from Absorption
966 and Reflectance of Seagrass Leaves using Trios-Ramses Spectroradiometer in Nusa Lembongan and Pemuteran,
967 Bali. *Jurnal Penginderaan Jauh dan Pengolahan Data Citra Digital*, 17(2), 103-113.
968 <http://dx.doi.org/10.30536/j.pjpdcd.2020.v17.a3384>, 2020.
- 969 Irons, J. R. Dwyer, J. L. and Barsi, J. A.: The next Landsat satellite: the Landsat data continuity mission. *Remote*
970 *Sensing of Environment*, 122, 11–21. <https://doi.org/10.1016/j.rse.2011.08.026>, 2012.
- 971 Jackson, R. D., Pinter, P. J., Paul, J., Reginato, R. J., Robert, J. and Idso, S. B.: *Hand-Held Radiometry. Agricultural*
972 *Reviews and Manuals, ARM-W-19*; U.S. Department of Agriculture Science and Education Administration:
973 Phoenix, AZ, USA, 1980.
- 974 James, M. E. and Kalluri, S. N. V.: The Pathfinder AVHRR land data set: an improved coarse resolution data set for
975 terrestrial monitoring. *Int. Journal of Remote Sensing*, 15(17), 3347–3363, 1994.

- 976 Johnsen, G. and Sakshaug, E.: Biooptical characteristics of PSII and PSI in 33 species (13 pigment groups) of marine
977 phytoplankton, and the relevance for pulse amplitude-modulated and fast-repetition-rate fluorometry1. *Journal of*
978 *Phycology*, 43, 1236–1251, 2007.
- 979 Kibele, J.: Submerged habitats from space: Increasing map production capacity with new methods and software. PhD
980 Thesis, Institute of Marine Science, the University of Auckland, New-Zeeland, 179 pp, 2017.
- 981 Kirk, J. T. O.: Light and photosynthesis in aquatic ecosystems, 2nd edition. Cambridge university press, 509 pp.
982 <https://doi.org/10.1017/CBO9780511623370>, 1994.
- 983 Knight, E. and Kvaran, G.: Landsat-8 operational land imager design, characterization and performance. *Remote*
984 *Sensing*, 6(11), 10286–10305, 2014.
- 985 Knudby, A. and Nordlund, L.: Remote sensing of seagrasses in a patchy multi-species environment. *Int. Journal of*
986 *Remote Sensing*, 32(8), 2227–2244, 2011.
- 987 Kokaly, R. F., Despain, D. G., Clark, R. N. and Livo, K. E.: Mapping vegetation in Yellowstone National Park using
988 spectral feature analysis of AVIRIS data. *Remote Sensing of Environment*, 84, 437–456, 2003.
- 989 Komatsu, T., Hashim, M., Nurdin, N., Noiraksar, T., Prathep, A., Stankovic, M., Hoang-Son, T. P., Thu, P. M., Luong,
990 C. V., Wouthyzen, S., Phauk, S., Muslim, A. M., Yahya, N. N., Terauchi, G., Sagawa, T. and Ken-ichi
991 Hayashizaki, K.-H.: Practical mapping methods of seagrass beds by satellite remote sensing and ground trothing.
992 *Coastal Marine Science*, 43(1), 1–25, 2020.
- 993 Konstantinos, T., Spyridon, C. S., Apostolos, P. and Nikolaos, S.: The use of Sentinel-2 imagery for seagrass mapping:
994 Kalloni Gulf (Lesvos Island, Greece) case study. *Proceedings of the SPIE, Volume 9688, Fourth International*
995 *Conference on Remote Sensing and Geoinformation of the Environment (RSCy2016)*, 96881F.
996 [Doi:10.1117/12.2242887](https://doi.org/10.1117/12.2242887), <http://dx.doi.org/10.1117/12.2242887>, 2016.
- 997 Kovacs, E., Roelfsema, C., Lyons, M., Zhao, S. and Phinn, S.: Seagrass habitat mapping: how do Landsat 8 OLI,
998 Sentinel-2, ZY-3A, and Worldview-3 perform? *Remote Sensing Letters*, 9(7), 686–695, 2018.
- 999 Larkum, A. W. D., Orth, R. J. and Duarte, C. M.: Seagrasses: Biology, ecology and conservation. *Seagrasses: Biology,*
1000 *Ecology and Conservation*. <https://doi.org/10.1007/978-1-4020-2983-7>, 2006.
- 1001 Leleu, K., Alban, F., Pelletier, D., Charbonnel, E., Letourneur, Y. and Boudouresque, C.F.: Fishers' perceptions as
1002 indicators of the performance of Marine Protected Areas (MPAs). *Marine Policy*, 36(2), 414-422.
1003 <https://doi.org/10.1016/j.marpol.2011.06.002>, 2012.
- 1004 Li, J. and Chen, B.: Global Revisit Interval Analysis of Landsat-8 -9 and Sentinel-2A-2B Data for Terrestrial
1005 Monitoring. *Sensors*, 20, 6631. <https://doi.org/10.3390/s20226631>, 2020.
- 1006 Li, J. and Roy, D. P.: A Global Analysis of Sentinel-2A, Sentinel-2B and Landsat-8 Data Revisit Intervals and
1007 Implications for Terrestrial Monitoring. *Remote Sensing*, 9, 902. DOI: 10.3390/rs9090902, 2017.
- 1008 Li, S., Ganguly, S., Dungan, J. L., Wang, W. L. and Nemani, R. R.: Sentinel-2 MSI Radiometric Characterization and
1009 Cross-Calibration with Landsat-8 OLI. *Advances in Remote Sensing*, 6, 147-159. DOI : 10.4236/ars.2017.62011.,
1010 2017.
- 1011 Li, R., Liu, J.-K., Sukcharoenpong, A., Yuan, J., Zhu, H. and Zhang, S.: A Systematic Approach toward Detection of
1012 Seagrass Patches from Hyperspectral Imagery, *Marine Geodesy*, 35(3), 271-286, 2012.

- 1013 Li, S.: Seagrass Mapping and Human Impact Evaluation Using Remote Sensing Imagery at Core Banks, North
1014 Carolina. Duke University, 2018.
- 1015 Lin, C., Gong, Z. and Zhao, W.: The extraction of wetland hydrophytes types based on medium resolution TM data.
1016 *Shengtai Xuebao/Acta Ecologica Sinica*, 30(23), 6460–6469, 2010.
- 1017 Loveland, T. R. and Dwyer, J. L.: Landsat: Building a strong future. *Remote Sensing of Environment*, 122, 22–29.
1018 <https://doi.org/10.1016/j.rse.2011.09.022>, 2012.
- 1019 Lyimo, L. D.: Carbon sequestration processes in tropical seagrass beds. PhD Thesis, Department of Ecology,
1020 Environment and Plant Sciences, Stockholm University, Sweden, 2016.
- 1021 Lyons M. B., Phinn S. R. and Roelfsema C. M.: Integrating Quickbird Multi-Spectral Satellite and Field Data:
1022 Mapping Bathymetry, Seagrass Cover, Seagrass Species and Change in Moreton Bay, Australia in 2004 and 2007.
1023 *Remote Sensing*, 3, 42-64. doi:<http://dx.doi.org/10.3390/rs3010042>., 2011.
- 1024 Lyons, M. B., Phinn, S. R. and Roelfsema, C. M.: Long term land cover and seagrass mapping using Landsat and
1025 object-based image analysis from 1972 to 2010 in the coastal environment of South East Queensland, Australia.
1026 *ISPRS Journal of Photogrammetry and Remote Sensing*, 71, 34–46, 2012.
- 1027 Lyons, M. B., Roelfsema, C. M., and Phinn, S. R.: Towards understanding temporal and spatial dynamics of seagrass
1028 landscapes using time-series remote sensing. *Estuarine, Coastal and Shelf Science*, 20, 42–53, 2013.
- 1029 Mandanici, E. and Bitelli, G.: Preliminary Comparison of Sentinel-2 and Landsat 8 Imagery for a Combined Use.
1030 *Remote Sensing*, 8, 1014, 2016. DOI:10.3390/rs8121014., 2016.
- 1031 Manevski, K., Manakos, I., Petropoulos, G. P. and Kalaitzidis, C.: Discrimination of common Mediterranean plant
1032 species using field Spectroradiometry. *Int. J. of Applied Earth Observation and Geoinformation*, 13, 922–933,
1033 2011.
- 1034 Marcello, J., Eugenio, F., Martín, J. and Marqués, F.: Seabed Mapping in Coastal Shallow Waters Using High
1035 Resolution Multispectral and Hyperspectral Imagery. *Remote Sensing*, 10, 1208. DOI:10.3390/rs10081208, 2018.
- 1036 Markham, B., Barsi, J., Kvaran, G., Ong, L., Kaita, E., Biggar, S., Czapla-Myers, J., Mishra, N. and Helder, D.:
1037 Landsat-8 Operational Land Imager Radiometric Calibration and Stability. *Remote Sensing*, 6(12), 12275-12308.
1038 <https://doi.org/10.3390/rs61212275>, 2014.
- 1039 Markham, B., Jenstrom, D., Masek, J. G., Dabney, P., Pedelty, J. A., Barsi, J.A. and Montanaro, M.: Landsat 9: Status
1040 and plans. In *Earth Observing Systems XXI; International Society for Optics and Photonics: San Diego, CA, USA;*
1041 *Volume 9972*, p. 99720G, 2016.
- 1042 Mcfeeters, S. K.: The use of the normalized difference water index (NDWI) in the delineation of open water features.
1043 *Int. Journal of Remote Sensing*, 17, 1425-1432, 1996.
- 1044 Meehan, A. J., Williams, R. J. and Watford, F. A.: Detecting Trends in Seagrass Abundance Using Aerial Photograph
1045 Interpretation: Problems Arising with the Evolution of Mapping Methods. *Estuaries*, 28(3), 462-472, 2005.

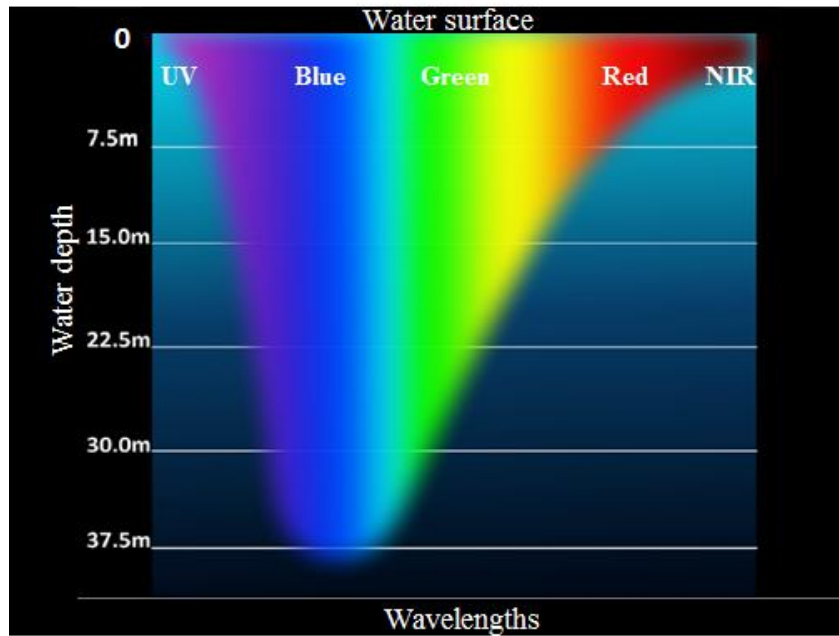
- 1046 Mount, R. E.: Rapid monitoring of extent and condition of seagrass habitats with aerial photography “mega-quadrats.
1047 Journal of Spatial Science, 52 (1), 105-119, 2007.
- 1048 Morrison, M. A., Lowe, M. L., Grant, C. M., Smith, P. J., Carbines, G., Reed, J., Bury, S. J. and Brown, J. (2014)
1049 Seagrass meadows as biodiversity and productivity hotspots. New Zealand Aquatic Environment and Biodiversity,
1050 Report No. 137, 151 pages. <http://www.mpi.govt.nz/news-resources/publications.aspx>, 2014.
- 1051 Mumby, P. J., Green, E. P., Edwards, A. J. and Clark, C. D.: Measurement of Seagrass Standing Crop using Satellite
1052 and Digital Airborne Remote Sensing. Marine Ecology Progress Series, 159, 51-60, 1997.
- 1053 NASA (2014) Landsat-8 Instruments. Available online (accessed on 18 March 2021):
1054 http://www.nasa.gov/mission_pages/landsat/spacecraft/index.html, 2014.
- 1055 NASA: Landsat-9 Mission Details. Available online (accessed on 18 March 2021).
1056 <https://landsat.gsfc.nasa.gov/landsat-9/landsat-9-mission-details/>, 2019.
- 1057 NASA: Landsat-9 overview, continuity the legacy - 2021 and beyond. [https://landsat.gsfc.nasa.gov/landsat-9/landsat-](https://landsat.gsfc.nasa.gov/landsat-9/landsat-9-overview)
1058 [9-overview](https://landsat.gsfc.nasa.gov/landsat-9/landsat-9-overview), 2021.
- 1059 Naser, H.: Human Impacts on Marine Biodiversity: Macro-benthos in Bahrain, Arabian Gulf. Chapter 7 (pp. 109-126)
1060 in “The Importance of Biological Interactions in the Study of Biodiversity. Edited by J. LÃ³pez-Pujol, ISBN: 978-
1061 953-307-751-2. Published by InTech, 390 pp, 2011
- 1062 Neckles, H. A., Kopp, B. S., Peterson, B. J. and Pooler, P. S.: Integrating Scales of Seagrass Monitoring to Meet
1063 Conservation Needs. Estuaries and Coasts, 35(1), 23-46, 2012.
- 1064 Novak, A. B and Short, F. T.: Submerged Aquatic Vegetation: Seagrasses. Encyclopedia of Natural Resources, 9
1065 pages. DOI: 10.1081/E-ENRW-120047540, 2014.
- 1066 Onuf, C. P.: Seagrasses, dredging and light in Laguna Madre, Texas, U.S.A.: Estuarine, Coastal and Shelf Science,
1067 39, 75-91, 1994.
- 1068 Orth, R. J., Carruthers, T. J. B., Dennison, W. C., Duarte, C. M., Fourqurean, J. W., Heck, K. L., Hughes, A. R.,
1069 Kendrick, G. A., Kenworthy, W. J., Olyarnik, S. Short, F. T., Waycott, M. and Williams, S. L.: A Global Crisis
1070 for Seagrass Ecosystems. Bioscience, 56(12), 987–996. [https://doi.org/10.1641/0006-](https://doi.org/10.1641/0006-3568(2006)56[987:AGCFSE]2.0.CO;2)
1071 [3568\(2006\)56\[987:AGCFSE\]2.0.CO;2](https://doi.org/10.1641/0006-3568(2006)56[987:AGCFSE]2.0.CO;2), 2006.
- 1072 Pasqualini, V., Pergent-Martini, C., Pergent, G., Agreil, M., Skoufas, G., Sourbes, L. and Tsirika, A.: Use of SPOT 5
1073 for mapping seagrasses: An application to Posidonia oceanica. Remote Sensing of Environment, 94(1), 39-45,
1074 2005.
- 1075 Peneva, E., Griffith, J. A. and Carter, G. A.: Seagrass mapping in the northern Gulf of Mexico using airborne
1076 hyperspectral imagery: a comparison of classification methods. Journal of Coastal Research, 24(4), 850–856, 2008.
- 1077 Perez, D., Islam, K., Hill, V., Zimmerman, R., Schaeffer, B., Shen, Y. and Li, J.: Quantifying Seagrass Distribution
1078 in Coastal Water with Deep Learning Models. Remote Sensing, 12, 1581. DOI:10.3390/rs12101581, 2020.
- 1079 Peterson, B. J. and Fourqurean, J. W.: Large-scale patterns in seagrass (*Thalassia testudinum*) demographics in south
1080 Florida. Limnology and Oceanography, 46(5), 1077-1090, 2001.

- 1081 Phinn, S., Roelfsema, C., Dekker, A., Brando, V. and Anstee, J.: Mapping seagrass species, cover and biomass in
1082 shallow waters: An assessment of satellite multispectral and airborne hyper-spectral imaging systems in Moreton
1083 Bay (Australia). *Remote Sensing of Environment*, 112(8), 3413-3425, 2008.
- 1084 Preen, A.: Distribution, abundance and conservation status of dugongs and dolphins in the southern and western
1085 Arabian Gulf. *Biological Conservation*, 118(2), 205-218, 2004.
- 1086 Pu, R., Bell, S., Baggett, L., Meyer, C. and Zhao, Y.: Discrimination of Seagrass Species and Cover Classes with *in*
1087 *situ* Hyperspectral Data. *Journal of Coastal Research*, 28(6),1330-1344, 2012.
- 1088 Richardson, A. J. and Wiegand, C. L.: Distinguishing vegetation from soil background information. *Photogrammetric*
1089 *Engineering and Remote Sensing*, 43(12), 1541-1552, 1977.
- 1090 Roelfsema, C. M., Lyons, M., Kovacs, E. M., Maxwell, P., Saunders, M. I., Samper-Villarreal, J. and Phinn, S. R.:
1091 Multi-temporal mapping of seagrass cover, species and biomass: A semi-automated object based image analysis
1092 approach. *Remote Sensing of Environment*, 150, 172–187, 2014.
- 1093 Roelfsema, C. M., Phinn, S. R., Udy, N. and Maxwell, P.: An integrated field and remote sensing approach for
1094 mapping seagrass cover, Moreton Bay, Australia. *Journal of Spatial Science*, 54(1), 45–62.
1095 <https://doi.org/10.1080/14498596.2009.9635166>, 2009.
- 1096 Rouse, J. W., Haas, R. W., Schell, J. A., Deering, D. W., Harlan, J. C. (1974) Monitoring the vernal advancement and
1097 retrogradation (Greenwave effect) of natural vegetation. NASA/GSFC Type-III Final Report, Greenbelt,
1098 Maryland, U.S.A., 164 pp, 1974.
- 1099 Roy, D. P., Li, J., Zhang, H. K., Yan, L., Huang, H. and Li, Z.: Examination of Sentinel-2A multi-spectral instrument
1100 (MSI) reflectance anisotropy and the suitability of a general method to normalize MSI reflectance to nadir BRDF
1101 adjusted reflectance. *Remote Sensing of Environment*, 199, 25-38. <https://doi.org/10.1016/j.rse.2017.06.019>,
1102 2017.
- 1103 Roy, D., Zhang, H., Ju, J., Gomez-Dans, J., Lewis, P., Schaaf, C., Sun, Q., Li, J., Huang, H. and Kovalskyy, V.: A
1104 general method to normalize Landsat reflectance data to nadir BRDF adjusted reflectance. *Remote Sensing of*
1105 *Environment*, 176, 255–271. <https://doi.org/10.1016/j.rse.2016.01.023>, 2016.
- 1106 Roy, D. P., Wulder, M. A., Loveland, T. R., Woodcock, C. E., Allen, R. G., Anderson, M. C., Helder, D., Irons, J. R.,
1107 Johnson, D. M., Kennedy, R., Scambos, T. A., Schaaf, C. B., Schott, J. R., Sheng, Y., Vermote, E. F., Belward, A.
1108 S., Bindschadler, R., Cohen, W. B., Gao, F., Hipple, J. D., Hostert, P., Huntington, J., Justice, C. O., Kilic, A.,
1109 Kovalskyy, V., Lee, Z. P., Lyburner, L., Masek, J. G., McCorkel, J., Shuai, Y., Trezza, R., Vogelmann, J.,
1110 Wynne, R. H. and Zhu, Z.: Landsat-8: science and product vision for terrestrial global change research. *Remote*
1111 *Sensing of Environment*, 145, 154–172. <https://doi.org/10.1016/j.rse.2014.02.001>, 2014.
- 1112 Saarman, E., Gleason, M., Ugoretz, J., Airamé, S., Carr, M., Fox, E., Frimodig, A., Mason, T. and Vasques, J.: The
1113 role of science in supporting marine protected area network planning and design in California, *Ocean and Coastal*
1114 *Management*, 74, 45-56. <https://doi.org/10.1016/j.ocecoaman.2012.08.021>, 2013.
- 1115 Sandmeier, St., Muller, Ch., Hosgood, B. and Andreoli, G.: Sensitivity Analysis and quality Assessment of Laboratory
1116 BRDF Data. *Remote Sensing of Environment*, 64, 176-191, 1998.

- 1117 Short, F. T. and Wyllie-Echeverria, S.: Natural and human-induced disturbance of seagrasses. *Environ. Conserv.*, 23,
1118 17-27, 1996.
- 1119 Short, F. T. and Coles, R.: *Global Seagrass Research Methods*. Elsevier Publishing, The Netherlands, 482 pp, 2001.
- 1120 Short, F. T., Polidoro, B., Livingstone, S. R., Carpenter, K. E., Bandeira, S., Bujang, J. S., Calumpong, H. P.,
1121 Carruthers, T. J. B., Coles, R. G., Dennison, W. C., Erfemeijer, P. L. A., Fortes, M. D., Freeman, A. S., Jagtap,
1122 T. G., Kamal-Abu-Hena, M., Kendrick, G. A., Kenworthy, W. J., La-Nafie, Y. A., Nasution, I. M., Orth, R. J.,
1123 Prathep, A., Sanciangco, J. C., Tussenbroek, B. V., Vergara, S. G., Waycott, M. W. and Zieman, J. C.: Extinction
1124 risk assessment of the world's seagrass species. *Biological Conservation*, 144(7), 1961–1971.
1125 <https://doi.org/10.1016/j.biocon.2011.04.010>, 2011.
- 1126 Silva, T. S. F., Costa, M. P. F., Melack, J. M., and Novo, E. M. L. M.: Remote sensing of aquatic vegetation: Theory
1127 and applications. *Environmental Monitoring and Assessment*, 140(1-3), 131-145. [https://doi.org/10.1007/s10661-](https://doi.org/10.1007/s10661-007-9855-3)
1128 [007-9855-3](https://doi.org/10.1007/s10661-007-9855-3), 2008.
- 1129 Skakun, S., Roger, J.-C., Vermote, E. F., Masek, J. G. and Justice, C. O.: Automatic sub-pixel co-registration of
1130 Landsat-8 Operational Land Imager and Sentinel-2A Multi-Spectral Instrument images using phase correlation
1131 and machine learning based mapping. *Int. J. of Digital Earth*, 10(12), 1253-1269.
1132 <http://dx.doi.org/10.1080/17538947.2017.1304586>, 2017.
- 1133 Slater, P. N.: *Remote Sensing - Optics and Optical System*. Addison-Wesley, reading, MA, 575 pp. 1980.
- 1134 Teillet, P. M. and Santer, R.: Terrain Elevation and Sensor Altitude Dependence in a Semi-Analytical Atmospheric
1135 Code". *Canadian J. of Remote Sensing*, 17, 36-44, 1991.
- 1136 Thakur, Y. et al.: Sea Turtles. Chapter 9, pp. 165–177. In *Marine Environment and Resources of Abu Dhabi*, edited
1137 by T.Z. Al-Abdessalam, published by Environment Agency of Abu-Dhabi, UAE, 255 pp, 2007.
- 1138 Thorhaug, A., Richardson, A. D. and Berlyn, G. P.: Spectral reflectance of the seagrasses: *Thalassia testudinum*,
1139 *Halodule wrightii*, *Syringodium filiforme* and five marine algae. *Int. Journal of Remote Sensing*, 28(7), 1487–
1140 1501, 2007.
- 1141 Traganos, D.: Development of seagrass monitoring techniques using remote sensing data. PhD Thesis, Osnabrück
1142 University, Osnabrück in Lower Saxony, Germany, 199 pp, 2020.
- 1143 Uhrin, A. V. and Townsend, P. H.: Improved Seagrass Mapping Using Linear Spectral Unmixing of Aerial
1144 Photographs. *Estuarine, Coastal and Shelf Science*, 171, 11-22, 2016.
- 1145 Umamaheswari, R., Ramachandran, S. and Nobi, E. P.: Mapping the extend of seagrass meadows of Gulf of Mannar
1146 Biosphere Reserve, India using IRS ID satellite imagery. *Int. Journal of Biodiversity and Conservation*, 1(5), 187-
1147 193, 2009.
- 1148 Van-Der-Meera, F.: Analysis of spectral absorption features in hyperspectral imagery. *Int. J. Appl. Earth Observation*
1149 and Geoinformation, 5, 55–68, 2004.
- 1150 Van-der-Werff, H. and Van-der-Meer, F.: Sentinel-2A MSI and Landsat 8 OLI Provide Data Continuity for Geological
1151 Remote Sensing. *Remote Sensing*, 8, 883. <https://doi.org/10.3390/rs8110883>, 2016.

- 1152 Vermote, E., Justice, C., Claverie, M. and Franch, B.: Preliminary analysis of the performance of the Landsat 8/OLI
1153 land surface reflectance product. *Remote Sensing of Environment*, 185(2), 46–56.
1154 DOI: 10.1016/j.rse.2016.04.008, 2016.
- 1155 Villa, P., Bresciani, M., Braga, F. and Bolpagni, R.: Comparative Assessment of Broadband Vegetation Indices over
1156 Aquatic Vegetation. *IEEE Journal of Selected Topics in Applied Earth Observations and Remote Sensing*, 7(7),
1157 3117-3127, 2014.
- 1158 Villa, P., Mariano Bresciani, M., Braga, F. and Bolpagni, R.: Mapping Aquatic Vegetation through Remote Sensing
1159 Data: A Comparison of Vegetation Indices Performances. 6th EARSeL Workshop on Remote S. of the Coastal
1160 Zone, 7-8 June 2013, Matera, Italy, pp. 10-15, 2013.
- 1161 Wabnitz, C. C., Andréfouët, S., Torres-Pulliza, D., Muller-Karger, F. E. and Kramer, P. A.: Regional-scale seagrass
1162 habitat mapping in the Wider Caribbean region using Landsat sensors: Applications to conservation and ecology.
1163 *Remote Sensing of Environment*, 12(8), 3455-3467, 2008.
- 1164 Warren, C., Dupont, J., Abdel-Moati, M., Hobeichi, S., Palandro, D. and Purkis, S.: Remote sensing of Qatar nearshore
1165 habitats with perspectives for coastal management. *Marine Pollution Bulletin*, 105(2), 641-653.
1166 <https://doi.org/10.1016/j.marpolbul.2015.11.036>, 2016.
- 1167 Waycott, M., Duarte, C. M., Carruthers, T. J. B., Orth, R. J., Dennison, W. C., Olyarnik, S., Calladine, A.,
1168 Fourqurean, J. W., Heck Jr., K. L., Hughes, A. R., Kendrick, G. A., Kenworthy, W. J., Short, F. T. and Williams,
1169 S. L.: Accelerating loss of seagrasses across the globe threatens coastal ecosystems. *PNAS* July 28,
1170 2009; 106 (30) 12377-12381; www.pnas.org/cgi/doi/10.1073/pnas.0905620106, 2009.
- 1171 Wicaksono, P. and Hafizt, M.: Mapping Seagrass from Space: Addressing the Complexity of Seagrass LAI Mapping,
1172 *European Journal of Remote Sensing*, 46(1), 18-39. <http://dx.doi.org/10.5721/EuJRS20134602>, 2013.
- 1173 Wicaksono, P., Fauzan, M. A., Kumara, I. S. W., Yogyakarta, R. N., Lazuardi, W. and Zhafarina, Z.: Analysis of
1174 reflectance spectra of tropical seagrass species and their value for mapping using multispectral satellite images.
1175 *Int. Journal of Remote Sensing*, 40(23), 8955-8977. DOI: 10.1080/01431161.2019.1624866, 2019.
- 1176 Wicaksono, P., Kumara, I. S., Kamal, M., Fauzan, A. M., Zhafarina, Z., Nurswantoro, D. A. and Yogyakarta, R. N.:
1177 Multispectral Resampling of Seagrass Species Spectra: WorldView-2, Quickbird, Sentinel-2A, ASTER VNIR,
1178 and Landsat 8 OLI. The 5th Geoinformation Science Symposium 2017 (GSS 2017). *IOP Conf. Series: Earth and
1179 Environmental Science*, 98(2017), 012039. DOI:10.1088/1755-1315/98/1/012039, 2017.
- 1180 Willmott, C.J.: Some comments on the evaluation of model performance. *Bull. Am. Meteorol. Soc.*, 63, 1309-1313,
1181 1982.
- 1182 Wood, J. S.: Hyperspectral analysis of seagrass in Redfish Bay, Texas. Ph.D. Thesis, Texas A&M University-Corpus
1183 Christi, Corpus Christi, Texas (USA), 141 pp, 2012.
- 1184 Wulder, M. A., Hilker, T., White, J. C., Coops, N. C., Masek, J. G., Pflugmacher, D. and Crevier, Y.: Virtual
1185 constellations for global terrestrial monitoring. *Remote Sensing of Environment*, 170, 62–76.
1186 <https://doi.org/10.1016/j.rse.2015.09.001>, 2015.

- 1187 Yan, L., Roy, D.P., Li, Z., Zhang, H.K. and Huang, H.: Sentinel-2A multi-temporal misregistration characterization
1188 and an orbit-based sub-pixel registration methodology. *Remote Sensing of Environment*, 215, 495-506.
1189 <https://doi.org/10.1016/j.rse.2018.04.021>, 2018.
- 1190 Yang, D. and Yang, C.: Seagrass Distribution in China with Satellite Remote Sensing. Chapter 4 in *Remote Sensing*
1191 *of Planet Earth*, edited by Yann Chemin, pp. 75-94. ISBN: 978-953-307-919-6, InTech. Available from:
1192 [http://www.intechopen.com/books/remote-sensing-of-planet-earth/seagrass-distribution-in-china-with-](http://www.intechopen.com/books/remote-sensing-of-planet-earth/seagrass-distribution-in-china-with-remotesensing)
1193 [remotesensing](http://www.intechopen.com/books/remote-sensing-of-planet-earth/seagrass-distribution-in-china-with-remotesensing), 2012.
- 1194 Yang, D. and Yang, C.: Detection of seagrass distribution changes from 1991 to 2006 in Xincun Bay, Hainan, with
1195 satellite remote sensing. *Sensors*, 9(2), 830-844, 2009.
- 1196 Zhang, H. K. and Roy, D. P.: Computationally inexpensive Landsat-8 operational land imager (OLI) pan-sharpening.
1197 *Remote Sensing*, 8 (3), 180, 2016.
- 1198 Zhang, H. K., Roy, D. P., Yan, L., Li, Z., Huang, H., Vermote, E., Skakun, S. and Roger, J. C.: Characterization of
1199 Sentinel-2A and Landsat-8 top of atmosphere, surface, and nadir BRDF adjusted reflectance and NDVI
1200 differences. *Remote Sensing of Environment*, 215, 482-494. <https://doi.org/10.1016/j.rse.2018.04.031>, 2018.
- 1201 Zhao, D., Lv, M., Jiang, H., Cai, Y., Xu, D. and An, S.: Spatio-Temporal Variability of Aquatic Vegetation in Taihu
1202 Lake over the Past 30 Years. *PLoS ONE*, 8(6), 6–12. <https://doi.org/10.1371/journal.pone.0066365>, 2013.
- 1203 Zoffoli, M. L., Gernez, P., Rosa, P., Le-Bris, A., Brando, V. E., Barille, A.-L., Harin, N., Peters, S., Poser, K., Spaias,
1204 L., Peralta, G. and Barille, L.: Sentinel-2 remote sensing of *Zostera noltei*-dominated intertidal seagrass meadows.
1205 *Remote Sensing of Environment*, 251, 112020, 2020.
- 1206 Zorrilla, N. A., Vantrepotte, V., Ngoc, D.-D., Huybrechts, N. and Gardel, A.: Automated SWIR based empirical sun
1207 glint correction of Landsat 8-OLI data over coastal turbid water. *Optics Express*, 27(8), A294-A318.
1208 <https://doi.org/10.1364/OE.27.00A294>, 2019.
- 1209
1210
1211
1212
1213



1214

1215 **Figure 1.** Vertical penetration of electromagnetic spectrum in shallow water (adapted from: Morris, 2019),1216 https://commons.wikimedia.org/wiki/Category:Visible_spectrum_illustrations)

1217

1218

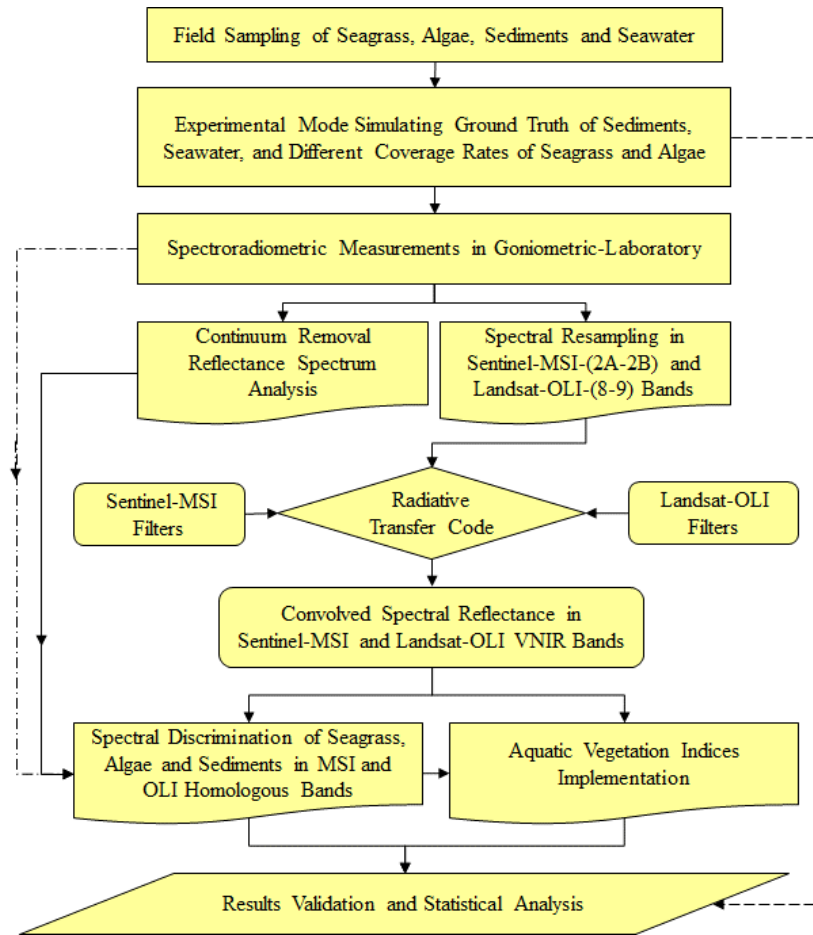
1219

1220

1221

1222

1223



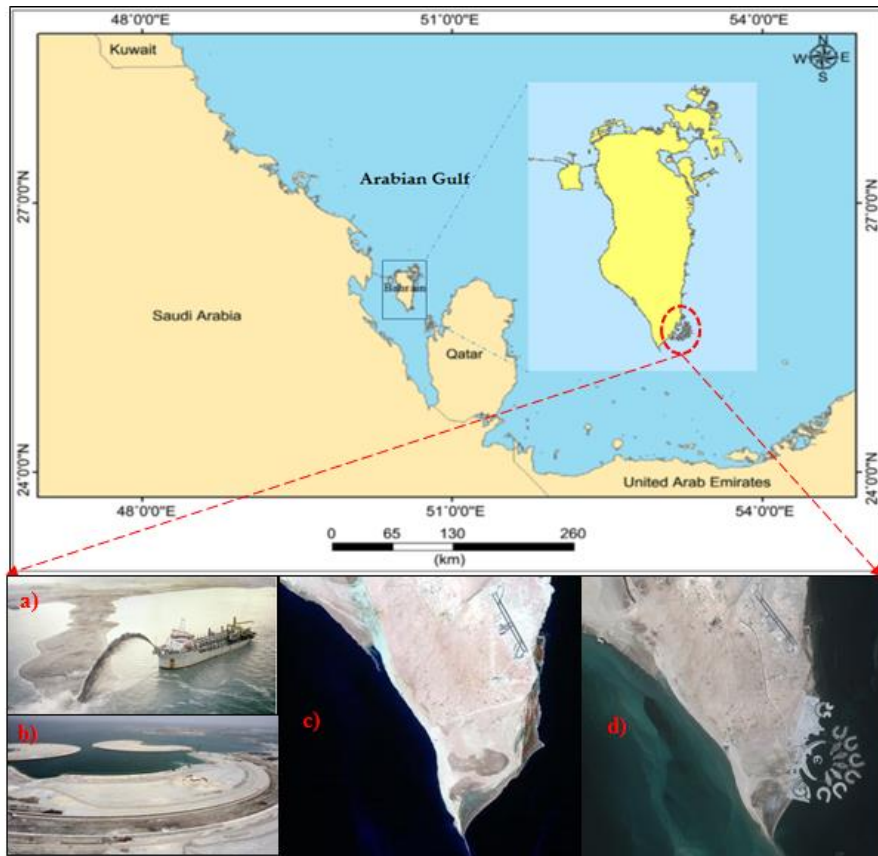
1224

1225 **Figure 2.** Methodology Flowchart

1226

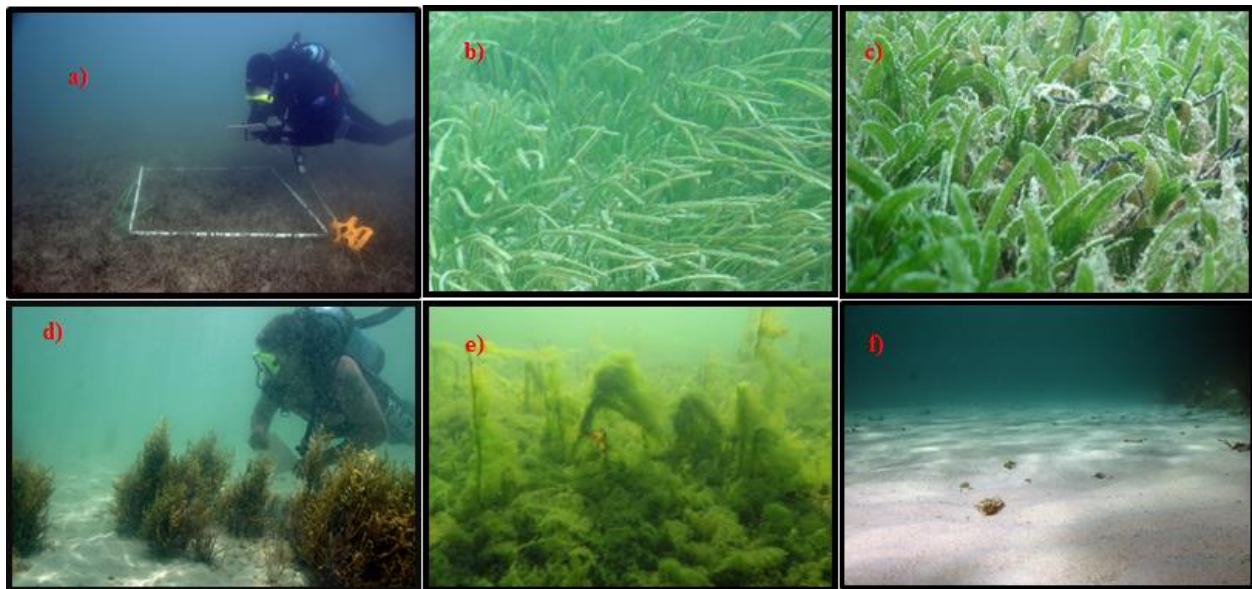
1227

1228



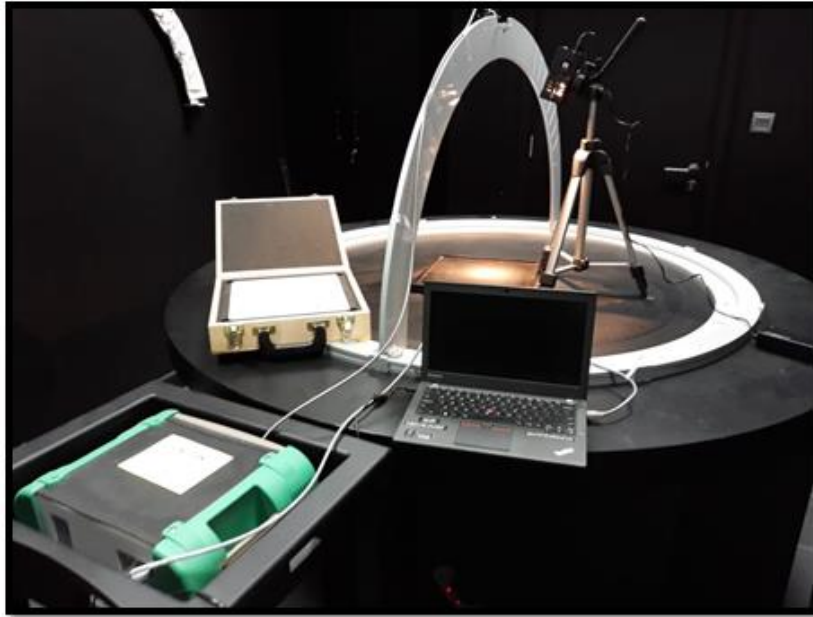
1229
 1230 **Figure 3.** Study site (Kingdom of Bahrain), photos illustrating dredging operations (a and b), and satellite images of
 1231 the south part of Bahrain before (c) and after (d) artificial islands construction.

1232



1233
 1234 **Figure 4.** Diver for sampling operation (a), and underwater photos of the considered seagrass and algae species: HU
 1235 (b), HS (c), BA (d), GA (e), and bright sediments (f).

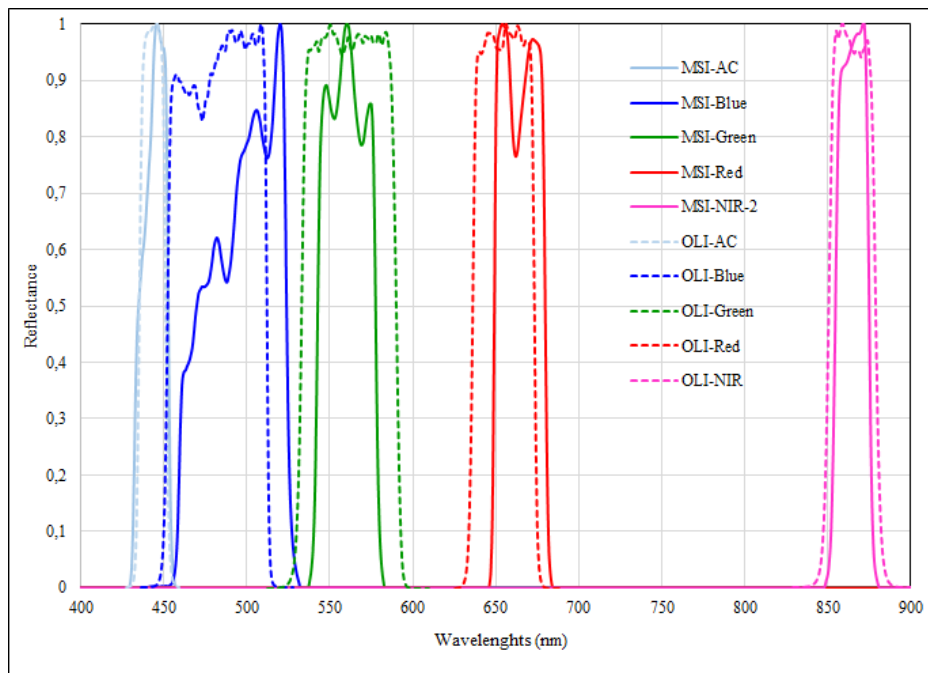
1236



1237

1238 **Figure 5:** Dark Goniometric-Laboratory for ASD measurements.

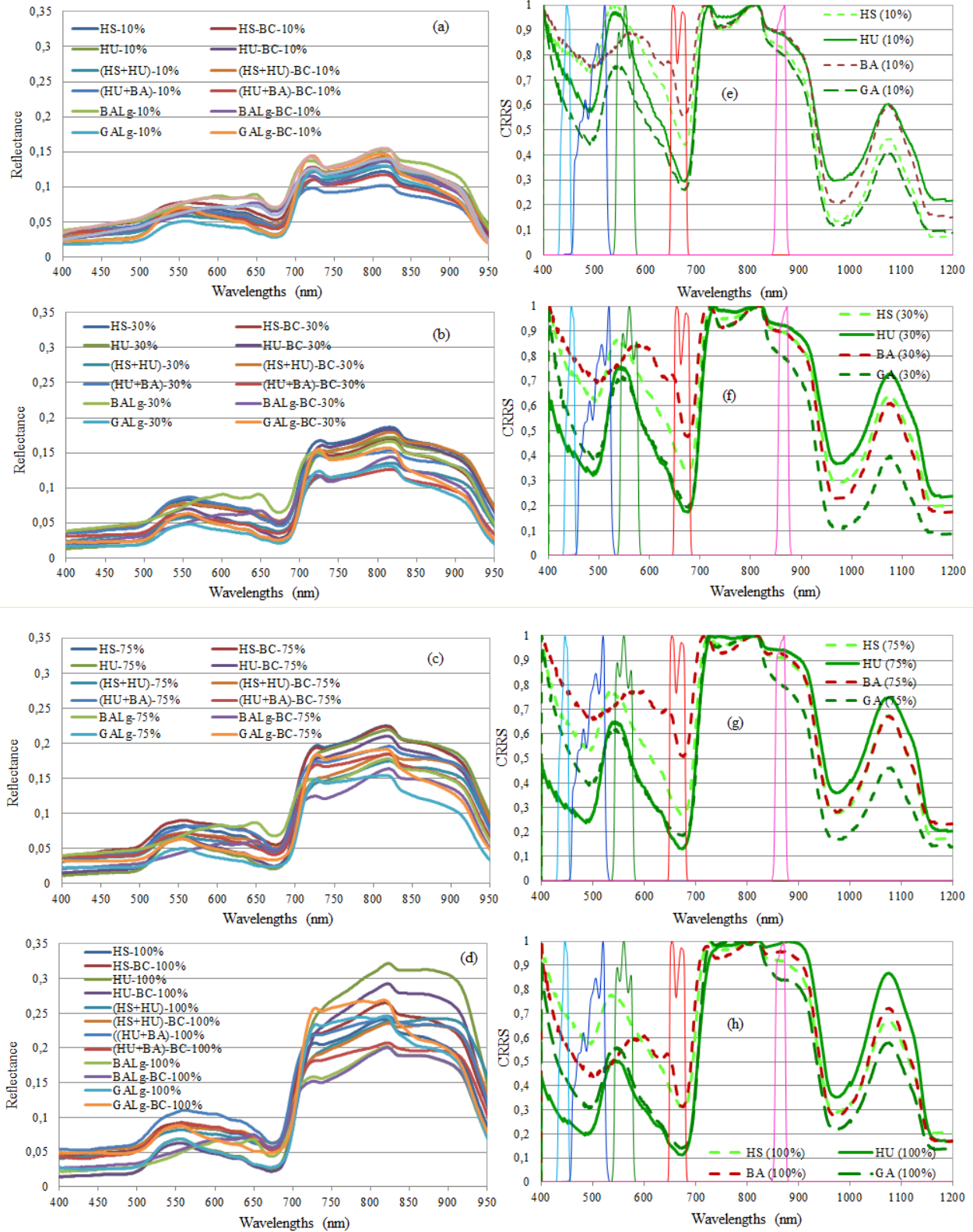
1239



1240

1241 **Figure 6.** Sentinel-MSI and Landsat-OLI relative spectral response profiles characterizing the filters of each spectral
1242 band in the VNIR.

1243



1244

1245

1246

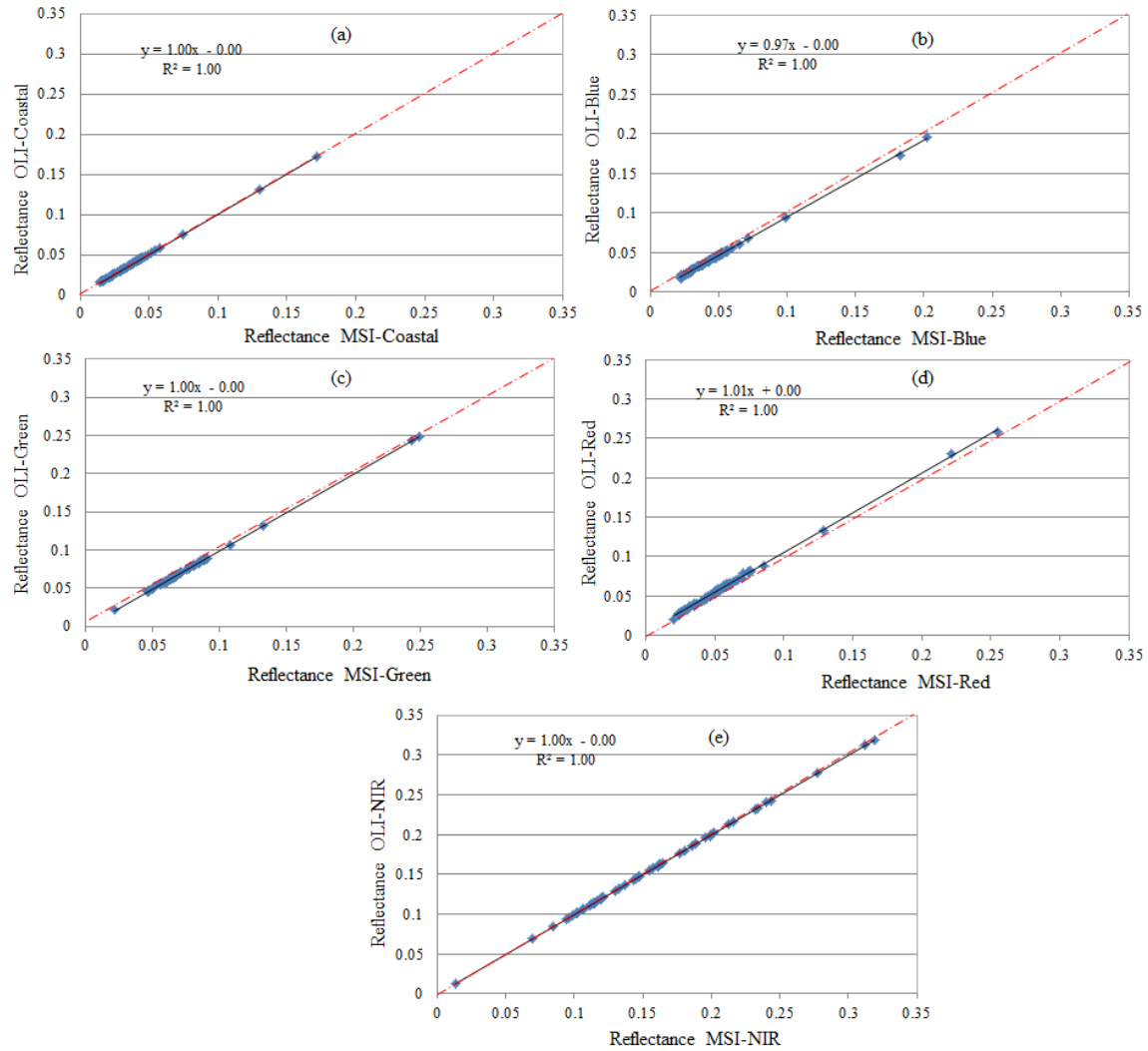
1247

Figure 7. Spectral signatures of seagrass and algae samples at different coverage rates (a: 10%, b: 30%, c: 75%, and d: 100%) and their CRRS transformations with the filters of Sentinel-MSI VNIR bands presented in Fig. 6.

1248

1249

1250



1251

1252 **Figure 8.** Scatter-plots of reflectances sampled and convolved in MSI and OLI homologous spectral bands.

1253

1254

1255

1256

1257

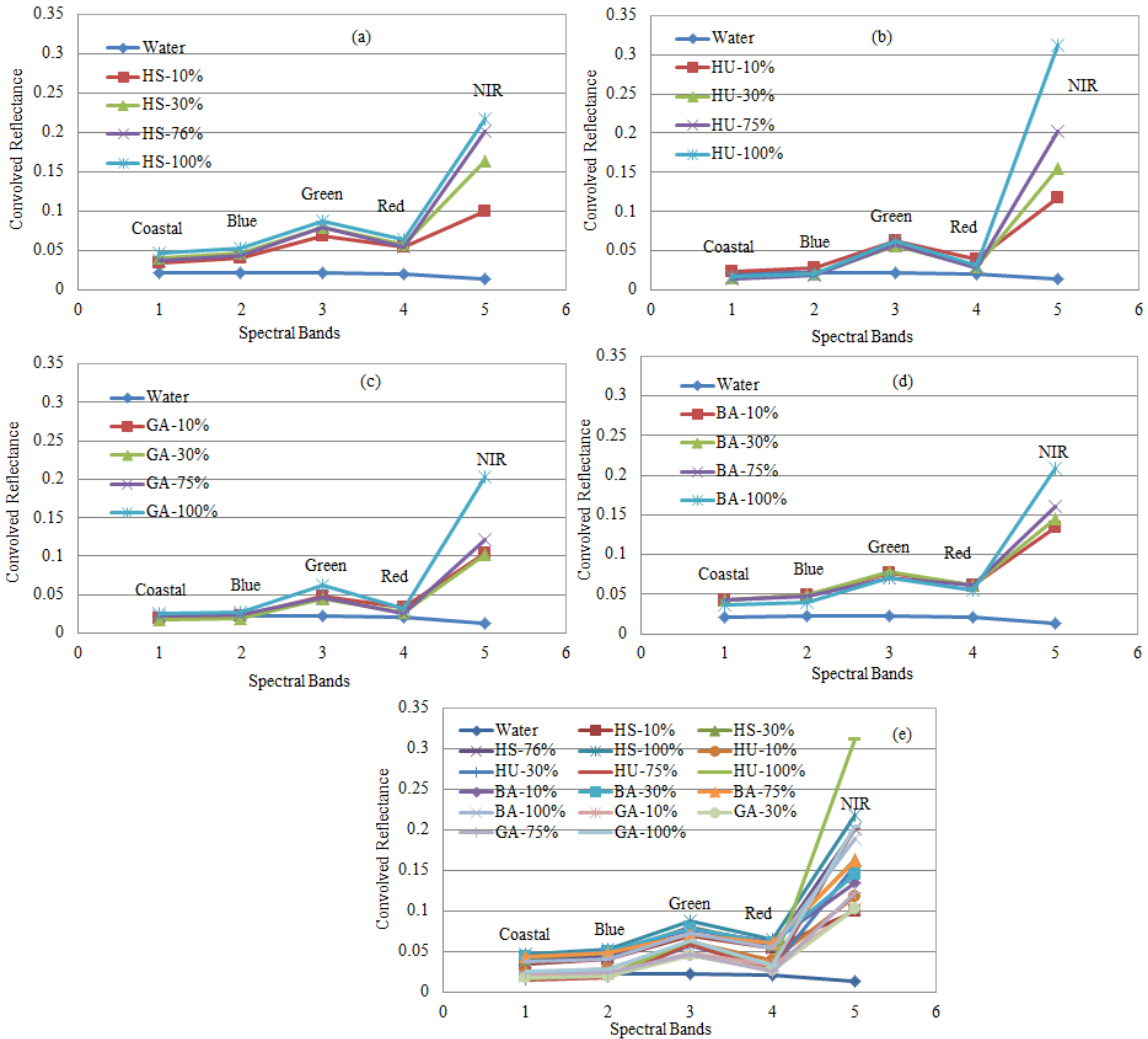
1258

1259

1260

1261

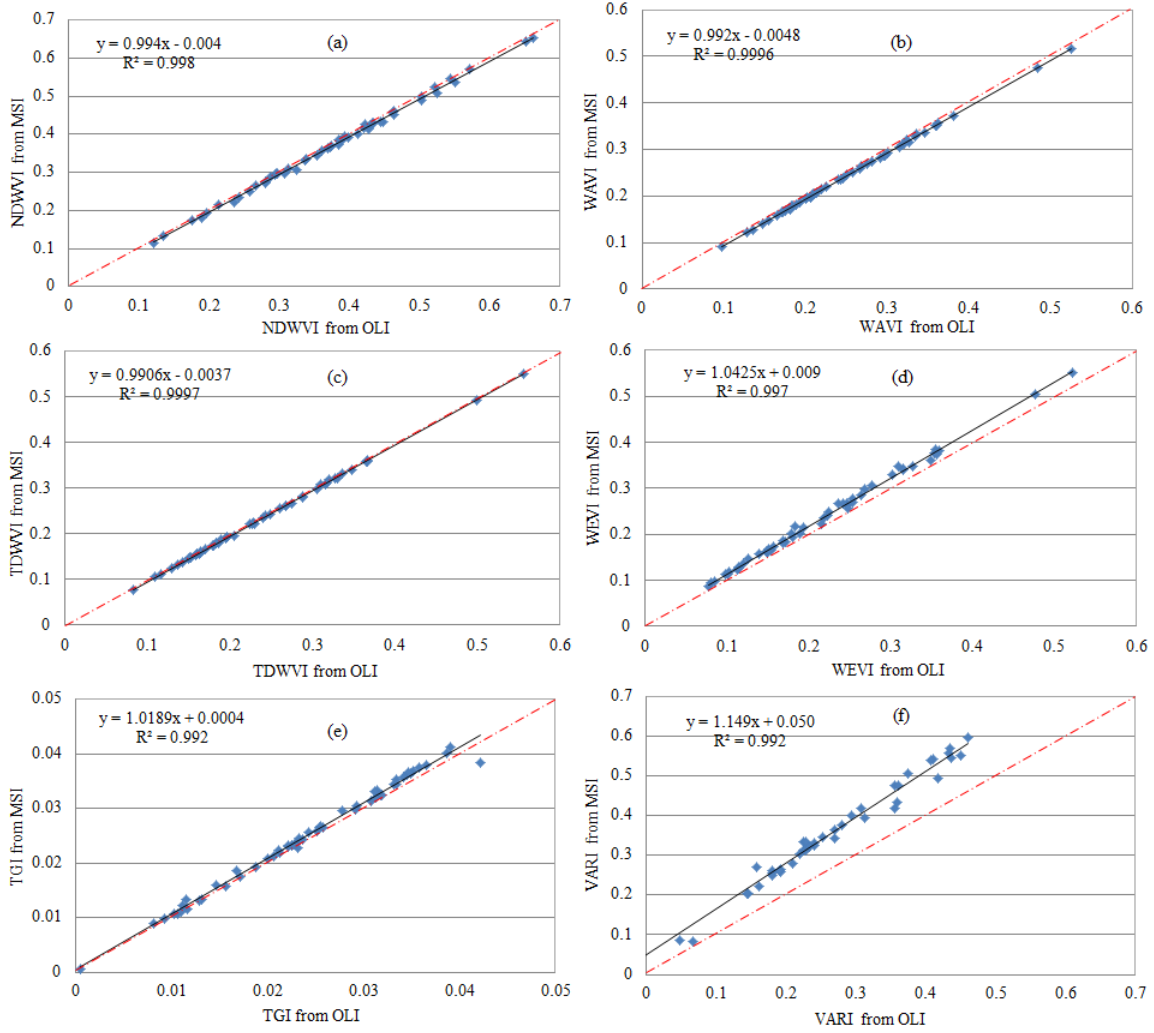
1262



1263

1264 **Figure 9.** Seagrass, algae, and seawater reflectances resampled and convolved in VNIR bands of Sentinel-MSI (or
 1265 Landsat-OLI): HS (a), HU (b), GA (c), BA (d), and all samples (e).

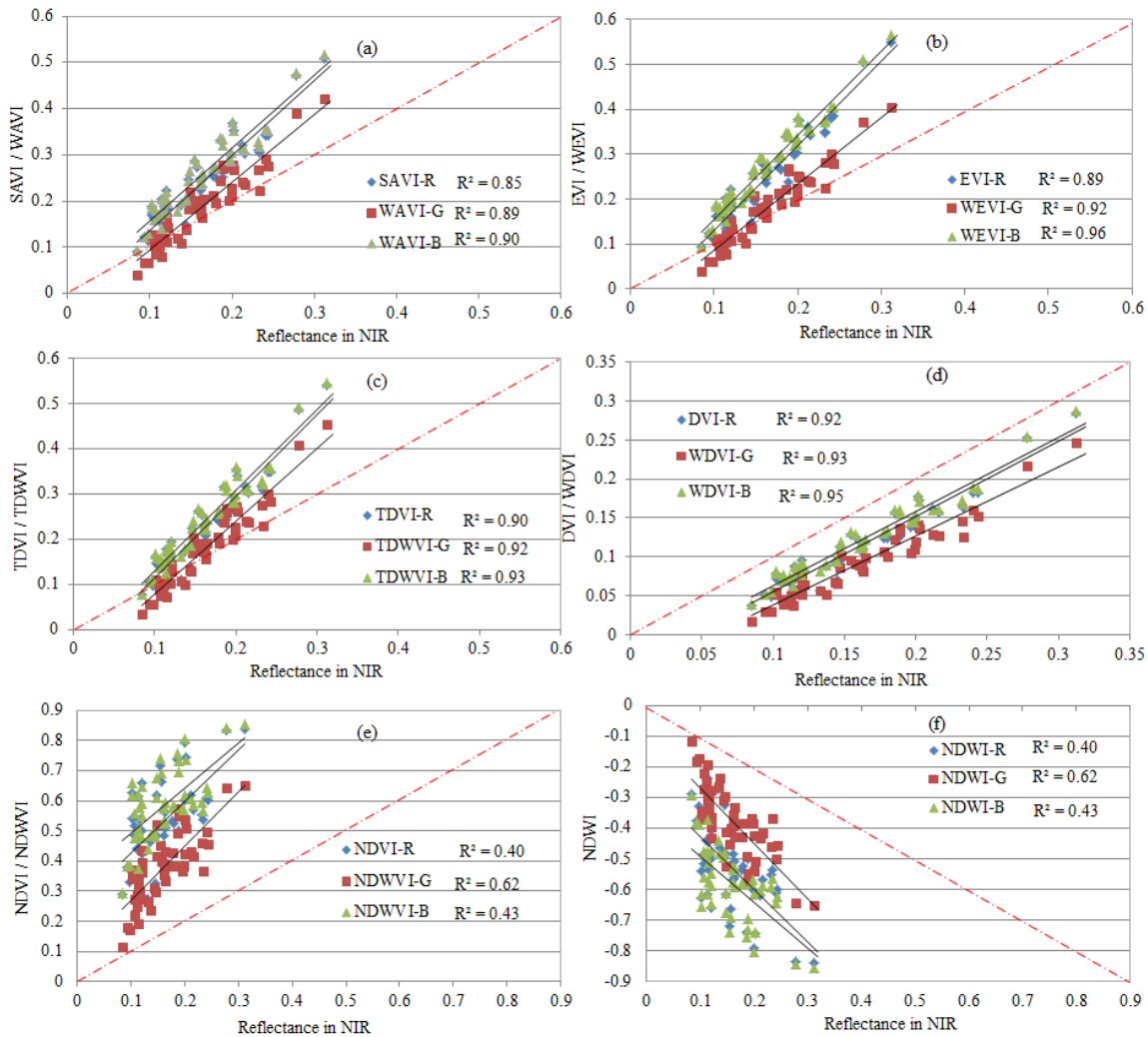
1266



1267

1268 **Figure 10.** Scatter-plots of homologous WVI derived from MSI and OLI simulated data.

1269



1270
 1271 **Figure 11.** Linear regressions ($p < 0.05$) between WVI and reflectance in NIR considering all samples, and integrating
 1272 the red, green, and blue bands.
 1273

1274 **Table 1.** The Sentinel-MSI and Landsat-OLI effective bandwidths and characteristics (λ = wavelength, SNR = signal
 1275 to noise ratio, $L_{ref}(\lambda)$ = reference radiance, $E_0(\lambda)$ = Extra-atmospheric irradiance,).

Spectral Bands	Sentinel-MSI					Landsat-OLI				
	λ Centre (nm)	$\Delta\lambda$ (nm)	Pixel Size (m)	SNR	$L_{ref}(\lambda)$ ($w/m^2/Sr/\mu m$)	λ Centre (nm)	$\Delta\lambda$ (nm)	Pixel Size (m)	SNR	$E_0(\lambda)$ ($w/m^2/\mu m$)
Coastal	443	20	60	129	129	443	16	30	130	1895.6
Blue	490	65	10	154	128	482	60	30	130	2004.6
Green	560	35	10	168	128	561	57	30	100	1820.7
Red	655	30	10	142	108	655	38	30	90	1549.4
NIR-2	865	20	20	72	52.5	865	28	30	90	951.2
SWIR-1	1609	85	20	100	4	1609	85	30	100	247.6
SWIR-2	2201	187	20	100	1.5	2201	187	30	100	85.5

1276

1277

1278

1279 **Table 2.** R^2 ($p < 0.05$) between vegetation indices integrating red, blue, and green bands and the reflectances in NIR
 1280 for all considered samples, and the RMSD between indices derived from MSI and OLI sensors data.

Index	Used band	R^2	RMSD* in %	Index	Used band	R^2	RMSD* in %	Index	Used band	R^2	RMSD* in %
NDVI	R	0.40	1.0	TDVI	R	0.90	0.3	DVI	R	0.92	0.2
	G	0.63	0.5		G	0.92	0.2		G	0.93	0.1
	B	0.43	1.0		B	0.93	0.2		B	0.95	0.1
SAVI	R	0.85	0.3	EVI	R	0.89	0.9	NDWI	R	0.40	1.0
	G	0.89	0.2		G	0.92	0.3		G	0.63	0.5
	B	0.90	0.2		B	0.96	0.3		B	0.43	1.0
TGI		0.20	0.1	Diff(G-B)		0.63	0.1	VARI		0.63	3.0

1281 * is the RMSD between indices derived from MSI and OLI simulated data. The bold type highlight the significant R^2 .

1282

1283